- Analytical and approximate formulations applicable to predict flexural stiffness reduction of stainless steel beam-columns are provided.
- Extension the formulations for evaluating the elastic second order effects to the inelastic range.
- Verification of Geometrically Nonlinear Analysis with stiffness reduction for the in-plane stability deign of stainless steel elements.

Geometrically Non-linear Analysis with stiffness reduction for the stability design of stainless steel structures: Application to members and planer frames

Yanfei Shen, Rolando Chacón

Department of Civil and Environmental Engineering, Universitat Politècnica de Catalunya, Barcelona 08034, Spain

Abstract:

This paper focuses on the development of beam-column flexural stiffness reduction factor (τ_{MN}) applicable to the in-plane stability design of stainless steel beam-columns and frames with compact cold-formed square and rectangular hollow sections. The proposed τ_{MN} accounts for the deleterious influence of material non-linearity, residual stresses and member out-of-straightness. The use of a Geometrically Non-linear Analysis (GNA) with the proposed τ_{MN} eliminates the need for member buckling strength checks and thus, only cross-sectional strength checks are required. The proposed approach, aligned to AISC standards, is aimed at facilitating greater and more efficient use of stainless steel.

Two types of τ_{MN} are proposed: analytical and approximate. The analytical τ_{MN} presumes knowing the maximum internal second order moment (M_{r2}) within a member. It is developed by means of extending the formulations for evaluating the elastic second order effects to the inelastic range. The accuracy of the analytical τ_{MN} is verified for beam-columns and sub-assemblages. Since in practical design M_{r2} is not known in advance, an approximate expression of τ_{MN}, which is more likely to be used relative to the analytical τ_{MN}, is proposed by fitting variables to the analytically determined $_{MN}$. The accuracy of the approximate τ_{MN} is verified for frames with different geometrical and loading configurations. Furthermore, the proposed approach is compared against the Direct Analysis Method (DM). Results show that, compared to the DM, GNA coupled with the approximate τ_{MN} provides improved estimations, since the proposed τ_{MN} can more accurately capture stiffness reduction resulted from material non-linearity and well capture additional second order effects due to material non-linearity.

Keywords: Geometrically Non-linear Analysis; stiffness reduction; second order effects; stability; stainless steel

Notation

λ_c : Column slenderness

Δ/h: Out-of-plumbness

δ/L: Out-of-straightness

τ_b: Flexural stiffness reduction factor derived from the CRC column strength curve

τ_M: Flexural stiffness reduction factor for beam with compact sections

τ_N: Flexural stiffness reduction factor derived from the AISC-based stainless steel column strength curve

τ_{MN} : Flexural stiffness reduction factor for beam-column with compact sections

$B_{1\text{-}E}$: Amplification factor evaluates P-δ effects on elastic beam-columns

$B_{1\text{-}P}$: Amplification factor evaluates P-δ effects on inelastic beam-columns

$B_{2\text{-}E}$: Amplification factor evaluates P-Δ effects (including P-δ effects) on elastic beam-columns

$B_{2\text{-}P}$: Amplification factor evaluates P-Δ effects (including P-δ effects) on inelastic beam-columns

C_m : Equivalent uniform moment factor

DM: Direct Analysis Method provided in AISC 360-16

GMNIA: Geometrically and Materially Non-linear Analysis with Imperfections

GNA: Geometrically Non-linear Analysis

GNA-τ_{MN} : Geometrically Non-linear Analysis with τ_{MN}

GNA-τ_N: Geometrically Non-linear Analysis with τ_N

K : Effective length factor of the column

K_{sw} : Second order sway effects factor provided in Eurocode 3: Part 1-1

LA: Linear Elastic Analysis

M_1 and M_2: Applied external end moments, $|M_1| \leq |M_2|$.

M_n : Nominal flexural strength

M_{r1}: Maximum internal first order moment within the member

M_{r2}: Maximum internal second order moment within the member

$M_{r2\text{-}E}$: Maximum internal second order elastic moment within the member

$M_{r2\text{-}P}$: Maximum internal second order inelastic moment within the member

$M_{r2\text{-}GMNIA}$: M_{r2} determined by GMNIA

$M_{r2\text{-}\tau MN}$: M_{r2} determined by GNA-τ_{MN}

$M_{r2\text{-}\tau N}$: M_{r2} determined by DM

$M_{u\text{-}GMNIA}$: Ultimate external moment of the member determined by GMNIA

M_P : Moment at full cross-section yielding

M_y : Moment at yielding of the extreme fiber

P_e : Elastic critical buckling strength of the member

P_{e1}: Elastic critical buckling strength (non-sway mode) of the member with K=1

P_{es}: Elastic critical buckling strength (sway mode) of the member with effective length (KL)

$P_{e\text{-}\tau N}$: Elastic critical buckling load determined by the reduced flexural stiffness: τ_N times EI

P_n: Nominal compressive strength

61 $P_{e^*\text{-story}}$: Elastic critical buckling (sway mode) strength of the story (without R_M)

62 P_{r1}: Maximum internal first order axial force within the member

63 P_{r2}: Maximum internal second order axial force within the member

64 $P_{r2\text{-}\tau MN}$: P_{r2} determined by GNA-τ_{MN}

65 $P_{r2\text{-}\tau N}$: P_{r2} determined by DM

66 $P_{r2\text{-GMNIA}}$: P_{r2} determined by GMNIA

67 P_{story}: Total vertical load transferred by the story (from Linear Elastic Analysis)

68 P_y: Cross-section yield strength

69 P_u: Ultimate axial load of the member

70 $P_{u\text{-GMNIA}}$: P_u determined by GMNIA

71 $P_{u\text{-}\tau MN}$: P_u determined by GNA-τ_{MN}

72 R_c: Demand-capacity ratio determined by interaction design equations provided in ASIC 360-16

73 $R_{c\text{-GMNIA}}$: R_c with second order axial force and moment determined by GMNIA

74 $R_{c\text{-}\tau MN}$: R_c with second order axial force and moment determined by GNA-τ_{MN}

75 $R_{c\text{-}\tau N}$: R_c with second order axial force and moment determined by DM

76 R_M: Factor accounts for P-δ effects on the global behavior of the structure

77 W_{el}: Elastic cross-section modulus

78 W_{pl}: Plastic cross-section modulus

79 **1. Introduction**

80 Using a Geometrically Nonlinear Analysis (GNA) coupled with stiffness reduction to determine internal forces and
81 moments for ultimate limit state design checks has become a significant alternative for member-based design. GNA with
82 stiffness reduction captures second order effects at system and member levels (P-Δ and P-δ), considers initial global sway
83 imperfection, and adopts reduced stiffness to account for the influence of material non-linearity and residual stresses. For
84 GNA coupled with stiffness reduction, initial member out-of-straightness (δ/L) can be accounted for by four ways:

85 - By geometrically modelling out-of-straightness directly
86 - By applying equivalent horizontal loads appropriately
87 - By reducing stiffness implicitly using reduction factors
88 - By checking bucking resistance of members.

89 A representative example of GNA with stiffness reduction is the Direct Analysis Method (DM). DM first appeared in AISC
90 360-05 [1] as an alternative to Effective Length Method (ELM) for frame stability design, was upgraded in AISC 360-10

[2] and reorganized in AISC 360-16 [3] as the primary method for frame stability design (ELM was moved to Appendix 7 of [3]).

Compared with ELM, a significant advantage of GNA with stiffness reduction is that it eliminates the need of calculating effective length of the column. The calculation of effective length factor (K) may be both difficult and inaccurate for geometrically irregular frames. Another main advantage is that it provides more accurate internal moment, which is a great concern for the design of connections. In most cases, GNA with stiffness reduction gives an improved representation of internal moments at member-based ultimate strength limit state [4-6], which is closer to the values obtained by more advanced analysis such as plastic-zone analysis.

Currently, comparable methods to GNA with stiffness reduction are provided in other design codes. Methods M3, M4, and M5 for elastic global analysis provided in EN 1993-1-1:2015 (E) [7], which is the next generation of EN 1993-1-1: 2005 [8], from less complex to more complex, depends on the type of second order effects and imperfections considered in global analysis. However, there is a significant difference between GNA with stiffness reduction and these other methods, as the former adopts reduced stiffness values. The reduction in stiffness will produce more deformations, which will in turn result in increased internal forces and moments due to second order effects.

AISC Design Guide 27, Structural Stainless Steel [9], which is aligned to AISC 360-16, provides guidance for the design of stainless steels structures [10]. It states that the GNA with stiffness reduction method (DM) can be a reference to stability design of stainless steel frames provided that the member strengths are determined in accordance with AISC-based provisions provided in [9]. DM in AISC 360-16 [3] conservatively adopts the maximum allowable out-of-plumbness (Δ/h) of 0.002 specified in [11] to account for initial global sway imperfection of the system. The influence of member out-of-straightness (δ/L) is considered by member buckling strength check where the column is taken as pinned at both ends (K=1). A general flexural stiffness reduction factor $0.8\tau_b$ is suggested in section C2.3 of AISC 360-16 [3]. The factor τ_b, derived from Column Research Council (CRC) column strength curve [12], is intended to account for partial yielding (accentuated by the presence of residual stresses) under high axial load [13]. The factor 0.8, originally proposed by Surovek-Maleck and White [14-15], accounts for additional stiffness reduction under combined axial loading and bending moment (Commentary on section C2.3 of AISC 360-16 [3]).

Although calibration studies have shown that the flexural stiffness reduction factor $0.8\tau_b$ is appropriate to stability design of carbon steel beam-columns and frames, it may not be appropriate to the stainless steel counterparts. Stainless steel is softer than carbon steel in the stress range of proportional limit and 0.2% proof strength, and column buckling curve of stainless steel differs from carbon steel. Therefore, to use GNA with stiffness reduction for the stability design of stainless steel members and frames, an appropriate stiffness reduction factor is needed.

Previous research on determination of beam-column flexural stiffness reduction factor is available for carbon steel. Kucukler et al. [6, 16], Kucukler and Gardner [17-19] developed a function of beam-column flexural stiffness reduction factor for using GNA to the stability design of in-plane carbon steel beam-columns and frames with compact sections. The main variables of the function include first order maximum axial force, first order maximum bending moment, column flexural stiffness reduction factor, beam flexural stiffness reduction factor, and a moment gradient factor C_m. In [6, 16-19], column stiffness reduction factor is derived from column buckling curves given in EN 1993-1-1: 2005 [8], while beam flexural stiffness reduction factor for beams sufficiently restrained against lateral-torsional buckling (LTB) under pure bending, is developed using a similar empirical formulation to the one proposed by Zubydan [20] for compact cross-sections subjected to combined axial loading and bending moment. For the proposed flexural stiffness reduction formulations in [6, 16-20] , strain-hardening after achieving full plastic strength of the cross-section is not considered and residual stresses pattern recommended by the European Convention for Construction Steelwork (ECCS) [21] is adopted for compact I or H sections.

Furthermore, White et al. [13] proposed a simple interpolation equation to represent beam-column flexural stiffness reduction factor (referred to as $\tau_{MN,White}$) for using direct buckling analysis to the stability design of carbon steel members and frames with I-sections. The general expression of the interpolation equation is $\tau_{MN,White} = \rho^*\tau_a(\theta/90^o) + \tau_{M,AISC}(1-\theta/90^o)$, where the angle θ represents the position of the current force point within a normalized interaction plot of the axial and moment strength ratios for a given cross-section. For the interpolation equation, ρ^* accounts for local buckling effects, and τ_a is derived from column buckling curves given in AISC 360-16 [3] and, while $\tau_{M,AISC}$ is derived from lateral-torsional buckling (LTB) curve of beams given in AISC 360-16 [3]. For using second order refined plastic hinge method to frame stability design, Kim and Chen [22] extended the column flexural stiffness reduction factor derived CRC column strength curve, to be applicable to beam-columns with compact I cross-sections.

Different to the above studies, in this paper, the formulation of beam-column flexural stiffness reduction factor (τ_{MN}) for stainless steel beam-columns and frames with compact cold-formed rectangular hollow section (RHS) and square hollow section (SHS) is developed through analytical and numerical study. Compact sections in the current paper, which are in accordance with AISC Design Guide 27, Structural Stainless Steel [9], refer to sections that are not prone to local buckling reductions. These sections effectively cover Class 1 and 2 in European notation and can develop full plastic moment resistance before local buckling occurs.

Two types of τ_{MN} formulations are proposed (analytical expression and approximate expression). The analytical expression of τ_{MN}, includes the unknown maximum internal second order moment (M_{r2}). It is developed by an extension of the formulations for evaluating second order elastic effects. The approximate expression of τ_{MN}, independent from M_{r2}, is

proposed by fitting relevant variables to the analytically determined expression. The proposed τ_{MN} accounts for member out-of-straightness, residual stresses and material non-linearity.

Besides developing flexural stiffness reduction factors that are applicable to stainless steel members, another contribution of this paper is that the formulations of evaluating second order elastic effects are extended to determine the maximum inelastic second order moment within beam-columns, through incorporating τ_{MN} into elastic critical buckling load. This contribution is presented in Section 5.

In the following sections of the paper, the adopted finite element modelling approach is first presented, followed by a brief description of the AISC-based interaction design curves for stainless steel members. Derivation of the column flexural stiffness reduction factor (τ_N) and of the beam flexural stiffness reduction factor (τ_M) are then presented in Section 4. Development and verification of the analytical τ_{MN} is presented in Section 5. Development and verification of the approximate τ_{MN} is presented in Section 6.

2. Numerical modelling

The in-plane structural behavior of stainless steel structures is studied through finite element (FE) analysis. Abaqus/Standard (implicit solver) [23] is employed for FE analysis. The simulations are performed with two-dimensional linear beam element (B21), which uses the shear-flexible Timoshenko formulation. The cross-section is defined as box section (without rounder corners). A B21 box section has 5 default Simpson integration points in the two walls of the section. Two iterative methods, the Newton method (load controlled) [24] and Arc-length method [25] are employed to compute the solution of nonlinear equilibrium equations. Based on preliminary mesh convergence study, the adopted mesh density is 100 elements per member. Spread of plasticity through cross-section and along member length is traced by a distributed plasticity approach.

2.1. Stress-strain curve of the material

The material behavior of stainless steel is modelled based on the nonlinear two-stage stress-strain curve provided in EN 1993-1-4:2015 [26], given by Eq.(1) and (2) and shown in Fig.1, which is essentially the expression proposed by Ramberg-Osgood [27].

$$\varepsilon = \frac{\sigma}{E} + 0.002\left(\frac{\sigma}{f_y}\right)^n \quad \text{for } \sigma \le f_y \tag{1}$$

$$\varepsilon = 0.002 + \frac{f_y}{E} + \frac{\sigma - f_y}{E_y} + \varepsilon_u\left(\frac{\sigma - f_y}{f_u - f_y}\right)^m \quad \text{for } f_y < \sigma \le f_u \tag{2}$$

where E is Young's Modulus; f_y is 0.2% proof stress; n is the first stage strain hardening exponent; E_y is the tangent modulus at the 0.2% proof stress; $E_y=E/(1+0.002nE/f_y)$; m is the second stage strain hardening exponent; ε_u is the ultimate strain; f_u is the ultimate stress.

The expression of the two-stage stress-strain curve involves three basic parameters (E, f_y, n) for $\sigma \leq f_y$ and three additional parameters (ε_u, f_u, m) for $\sigma > f_y$. The additional parameters can be determined in terms with E, f_y and n [27]. Although the full stage Ramberg-Osgood curve is adopted in FE modeling, the ultimate strengths from FE analysis in this paper are limited to full plastic strength of the cross-section, and thus strain hardening that results in strengths greater than the full plastic strength of the cross-section is not considered. Currently strain-hardening after the formation of first plastic hinge is not permitted to be considered in the stability design of stainless steel structures [26, 28-29], even though stainless steel has considerable strain hardening behavior.

The weighted material property method proposed by Hradil and Talja [30] is adopted to account for the enhanced material properties of the corner regions (including the extended area) in cold-formed stainless steel cross sections. In this method, the material parameters are weighted in accordance with the flat or corner area compared to the whole cross-section area, and the weighted average material properties are assigned to the whole cross-section. The study of Arrayago [31] showed that the weighted average material property method provided excellent results for cold-formed stainless steel columns, beams, and beam-columns with cold formed RHS and SHS. For FE models described in this paper, the considered enhancement amplitude for yield strength and ultimate strength of the corner regions are based on the available test data reported in [31-33].

2.2 Residual stresses

Residual stresses of cold formed cross-sections comprise bending residual stresses, membrane residual stresses, and layer residual stresses (for the case of thick plates) [34-35]. These stresses are developed when plastic deformation occurs in cold-working process such as uncoiling, leveling and rolling to form a section. Residual stress patterns for cold formed stainless steel box sections are found to be typically comparable to those for carbon steel box sections [34-38]. The report of Jandera and Machacek [38] showed that for global behavior of stainless steel members with box sections, the effect of through-thickness longitudinal bending residual stresses is dominant and the effect of other residual stress components is negligible. Similar conclusion for carbon steel members and frames with cold formed box sections has been reported in [34, 39]. Therefore, only longitudinal residual stresses are considered in this paper. Longitudinal residual stresses are accounted for by modifying the stress-strain curve, where the procedure of modifying the stress-strain curve is similar to the one presented in [39], and the amplitude of longitudinal residual stresses is based on the residual stress model suggested in [35].

2.3 Geometric imperfections

The maximum allowable out-of-plumbness (Δ/h) of 0.002 specified in [11] is adopted in FE modelling to account for initial sway imperfection, while the maximum allowable out-of-straightness (Δ/L) of 0.001 specified in [11] is adopted to account

for initial local member imperfection. For isolated sway-restrained members and sway-restrained sub-assemblages, out-of-straightness (δ/L) is modelled directly by introducing the same Eigenmode shape obtained from preliminary buckling analysis. Buckling analysis is conducted prior to GNA in the identical models. For sway permitted structures, instead of direct modelling geometric imperfection, the effects of out-of-plumpness (Δ/h) and out-of-straightness (δ/L) are accounted for by means of applying notional loads (equivalent horizontal loads). Notional loads are applied to the directions that produces the most destabilizing effect, where out-of-plumbness is modelled in the direction of sway deformation, while out-of-straightness is modelled in the mostly deformed direction obtained from a preliminary buckling analysis. The procedure of applying notional load is similar to the one presented by Ziemian [40]. To avoid additional shear force due to notional loads, corresponding horizontal reaction forces are applied.

2.4 Validation of finite element models

The developed FE models are validated against the experimental results on stainless steel beam-columns reported in [41]. The specimen S1-EC1 (SHS) and S3-EC1 (RHS), which are not susceptible to local buckling effects, are considered. The details of the dimensions and the weighted average material properties of the two specimens are shown in Table 1. L is the length of the specimen. D,W, and t are the depth, width, and thickness of the cross-section, respectively. δ_0 is the initial member bow imperfection. For the validation study, the full stage Ramberg-Osgood curves are adopted. In addition, longitudinal bending residual stresses are not modelled, since they are implicitly included in the tested material parameters. Comparison of the numerical results against experimental results for the two beam-columns is shown in Fig.2. It can be seen that the numerical results are in very close agreement with experimental results.

Table 1 Geometric and material parameters of the tested specimen reported in [41]

Specimen	Dimensions					Weighted average material properties					
	L (mm)	D (mm)	W (mm)	t (mm)	δ_0 (mm)	E (GPa)	f_y (MPa)	f_u (MPa)	ε_u (%)	n	m
S1-EC1	1495	80.1	80.3	3.9	1.25	173	539	587	5.8	8.8	2.6
S3-EC1	1500	80	40.2	3.8	0.89	183	529	554	2.5	12.9	2.7

3. AISC-based interaction design curves for stainless steel members

As the proposed approach is aligned to AISC standards, AISC-based interaction design equations, given by Eq. (3) and (4), are adopted in this paper. The two design equations are also adopted in AISC Design Guide 27 [9] for the design of stainless steel elements and frames. The equations are established mainly based on analyzed results of 82 second order inelastic beam-columns [42]. For stainless steel, the nominal compressive strength (P_n) of a column and nominal flexural strength (M_n) of a beam have to be determined in accordance with [9].

$$\frac{P_{r2}}{\phi_c P_n} + \frac{8}{9}\frac{M_{r2}}{\phi_b M_n} \leq 1 \qquad \text{for } \frac{P_{r2}}{\phi_c P_n} \geq 0.2 \tag{3}$$

$$\frac{P_{r2}}{2\,\phi_c P_n} + \frac{M_{r2}}{\phi_b M_n} \leq 1 \qquad \text{for } \frac{P_{r2}}{\phi_c P_n} < 0.2 \tag{4}$$

In Eq.(3) and (4), P_{r2} and M_{r2}, are the maximum internal second order axial force and moment, respectively; P_n and M_n are the nominal compressive strength and nominal flexural strength, respectively; for in-plane beam-columns with compact cross-sections, M_n is equal to full plastic bending moment (M_p); $M_p=W_{pl}f_y$; W_{pl} is plastic gross section modulus; ϕ_c is resistance factor for compression and ϕ_b for bending; $\phi_c=\phi_b=0.9$. The value of $P_{r2}/(\phi_c P_n)+8/9\ M_{r2}/(\phi_b M_n)$ or $P_{r2}/(2\ \phi_c P_n)+M_{r2}/(\phi_b M_n)$ is hereafter referred to as Demand-capacity ratio (R_c).

It should be noted that, for ultimate limit design checks, if internal axial forces and moments are determined by advanced analysis that considers rigorously second order effects (P-Δ and P-δ) and relevant initial geometric imperfections (out-of-plumbness, out-of-straightness), only cross-section strength check is needed and member buckling strength check is eliminated.

4. Flexural stiffness reduction factor for stainless steel columns and beams

In this section, column flexural stiffness reduction factor (τ_N) and beam flexural stiffness reduction factor (τ_M) are derived from stainless steel column strength curve and moment-curvature relationship, respectively. The accuracy of both τ_N and τ_M is subsequently verified.

4.1 Flexural stiffness reduction factor for stainless steel columns

The flexural stiffness reduction factor (τ_N) for cold-formed stainless steel columns with RHS and SHS is derived from stainless steel column strength curve provided in Section 5.3 of AISC design guide 27 [9]. This curve is established by modifying relevant coefficient of AISC LRFD carbon steel column strength curve and calibrated against experimental data. The AISC LRFD-based stainless steel column strength curve (for compact section), shown in Fig.3 (a), is given by:

When $\lambda_c \leq 1.2$ $\qquad P_n = 0.5^{\lambda_c^2} P_y$ (5)

When $\lambda_c > 1.2$ $\qquad P_n = 0.531 P_e = \frac{0.531}{\lambda_c^2} P_y$ (6)

where P_n is the nominal compressive strength; P_n is equal to the nominal global buckling strength for a column with compact section; λ_c is column slenderness; $\lambda_c=(P_y / P_e)\hat{}0.5$; P_e is the elastic critical buckling strength of a column with effective length factor (K); P_y is cross -section yield strength; $P_y=Af_y$; A is cross-section area; f_y is 0.2% proof stress. Eq. (5) corresponds to inelastic buckling while Eq. (6) corresponds to elastic buckling.

The derivation of the column stiffness reduction factor is based on Eq. (7), as illustrated in Fig.3 (b).

$$\tau_N = \frac{P_n}{0.531 P_e} \tag{7}$$

For the elastic buckling case, $\tau_N=1$. For the inelastic buckling case, τ_N is less than 1. Rewriting Eq. (7), the following equation for both elastic and inelastic buckling is obtained.

$$P_e = \frac{P_n}{0.531\tau_N} \quad (8)$$

Substituting $\lambda_c = (P_y / P_e)^{\wedge}0.5$ into Eq. (5) gives

$$P_n = 0.5^{\frac{P_y}{P_e}} P_y \quad (9)$$

Substituting Eq.(8) into Eq.(9) gives

$$\frac{P_n}{P_y} = 0.5^{\frac{0.531\tau_N P_y}{P_n}} \quad (10)$$

$$\ln\frac{P_n}{P_y} = 0.531\tau_N \frac{P_y}{P_n} \ln 0.5 \quad (11)$$

$$\tau_N = -2.717 \frac{P_n}{P_y} ln \frac{P_n}{P_y} \quad (12)$$

For λ_c=1.2, P_n/P_y=0.37. Thus

when $\frac{P_n}{P_y} \le 0.37$ $(\lambda_c \ge 1.2)$ $\tau_N = 1$ (13)

when $\frac{P_n}{P_y} > 0.37$ $(\lambda_c < 1.2)$ $\tau_N = -2.717 \frac{P_n}{P_y} ln \frac{P_n}{P_y}$ (14)

It should be noted that for the determination of τ_N under different axial load, the nominal compressive strength P_n should be replaced by the maximum internal axial force (P_{r1}) that corresponds to the applied axial load. Thus, the expression of τ_N is given by Eq. (15) and (16). A plot of τ_N against P_{r1}/P_y is shown in Fig. 4.

When $\frac{P_{r1}}{P_y} \le 0.37$ $\tau_N = 1$ (15)

When $\frac{P_{r1}}{P_y} > 0.37$ $\tau_N = -2.717 \frac{P_{r1}}{P_y} ln \frac{P_{r1}}{P_y}$ (16)

4.2 Verification of the column flexural stiffness reduction factor

The accuracy of the column flexural stiffness reduction factor (τ_N) for predicting the compressive strength of members subjected to axial load is assessed in this section. A total of 23 simply supported columns with section 120x80x6 (basic material parameters: E=175 GPa, f_y=350MPa and n=6) subjected to axial loads are studied. The applied axial load is factored load. The length of the columns varies from 50mm to 7000 mm. L= [50, 100, 200, 300, 350, 400, 450, 500, 600, 700, 1000, 1500, 2000, 2500, 3000, 3500, 4000, 4500, 5000, 5500, 6000, 6500, 7000](mm). For each column, Geometrically and Materially Non-linear Analysis with Imperfections (GMNIA), Linear Elastic Analysis (LA) and GNA with τ_N (GNA-τ_N) are conducted.

The procedure of verification is shown in Fig.5. Firstly, GMNIA is conducted to determine ultimate axil load (P_u) of the columns, where the introduced out-of-straightness is 0.001. P_u predicted by GMNIA is denoted by $P_{u\text{-GMNIA}}$. Secondly, LA is conducted to obtain the maximum first order axial force, where the applied load is $P_{u\text{-GMNIA}}$. The introduced out-of-

straightness is 0.001 in implementing LA. The maximum first order axial force obtained from LA is referred to as P_{r1}. For all the studied simply supported columns, P_{r1} is equal to $P_{u\text{-}GMNIA}$. τ_N is calculated according to Eq.(15) and (16). Lastly, GNA-τ_N is conducted to predict ultimate axil load of the columns. Ultimate axil load predicted by GNA-τ_N is denoted by $P_{u\text{-}\tau N}$. . It should be mentioned that, even though τ_N includes out-of-straightness of 0.001, an imperfection value much smaller than 0.001is introduced into the columns to ensure that these columns can buckle in GNA (columns without any imperfection would not buckle in GNA). If the proposed τ_N expression is "perfect", the ultimate axial load determined by GNA-τ_N should be equal to the ultimate axial load determined by GMNIA. The discrepancy between them shows the quality of τ_N.

It is found that, the ultimate load $P_{u\text{-}\tau N}$ of the simply supported columns predicted by GNA-τ_N matches the elastic critical buckling load determined by the reduced flexural stiffness (τ_N times EI).

The elastic critical buckling load ($P_{e\text{-}\tau N}$), shown in Fig.6, is given by

$$P_{e-\tau N} = \frac{\pi^2(\tau_N EI)}{(L)^2} \tag{17}$$

where EI is initial flexural stiffness; L is unbraced length of the column.

Comparison of predicted results from GNA-τ_N against those determined by GMNIA is shown in Fig.7, where the ultimate axial load (P_u) predicted by different methods is normalized by full cross-section yield strength (P_y). It is observed that the ultimate axial loads predicted by GNA-τ_N agree very well with those predicted by GMNIA. The discrepancy between $P_{u\text{-}\tau N}$ and $P_{u\text{-}GMNIA}$ relies on the ability of the adopted AISC LRFD-based stainless steel column strength curve to capture accurately the actual behavior of the studied columns. Since AISC LRFD-based stainless steel column strength curve provided in [9] is calibrated against experimental data, further verification of column flexural stiffness reduction factor (τ_N) for other columns is not needed.

4.3 Flexural stiffness reduction factor for stainless steel beams

Bending stiffness reduction for in-plane beams refers to influence of spread of plasticity through cross-section and along the member. Bending stiffness reduction factor (τ_M) can be determined by the ratio of tangent flexural stiffness $(EI)_t$ to the initial flexural stiffness EI, given by:

$$\tau_M = \frac{(EI)_t}{EI} = \frac{\frac{dM_{r1}}{d\kappa}}{EI} \tag{18}$$

where $dM_{r1}/d\kappa$ is derived from a moment-curvature (M-κ) curve.

The adopted moment-curvature relationship prior to outer fibers yielding is based on the moment-curvature relationship for stainless steel beams with cold formed RHS and SHS, proposed in [43]. It considers material non-linearity and it is fitted by an analytical expression similar to the Ramberg-Osgood equation. The moment-curvature relationship is given by

Eq.(19) (symbols are not identical to those employed in [43]).

$$\kappa = \frac{M_{r1}}{EI} + \left[\frac{2}{D}\left(\frac{f_y}{E} + 0.002\right) - \frac{M_y}{EI}\right]\left(\frac{M_{r1}}{M_y}\right)^{n-1} \quad (19)$$

In Eq. (19), EI is the initial flexural stiffness; D is the height of the cross-section; M_y is moment at yielding of the extreme fiber; $M_y=W_{el}f_y$; W_{el} is elastic gross section modulus. It should be mentioned that the cross-section already undergoes plastic straining before internal moment reaches to M_y, due to the nonlinear stress-strain behavior of stainless steel.

Eq.(19) is an implicit equation. Differentiating with respect to κ on both sides of this equation gives

$$\frac{dM_{r1}}{d\kappa} = \left[\frac{1}{EI} + (n-1)\frac{1}{M_y}\left(\frac{2}{D}\left(\frac{f_y}{E} + 0.002\right) - \frac{M_y}{EI}\right)\left(\frac{M_{r1}}{M_y}\right)^{n-2}\right]^{-1} \quad (20)$$

Substituting Eq. (20) into Eq. (18) gives

$$\tau_M = \left[1 + (n-1)\left(\frac{2}{DM_y}\frac{1}{(f_y I + 0.002EI)} - 1\right)\left(\frac{M_{r1}}{M_y}\right)^{n-2}\right]^{-1} \quad (21)$$

Substituting $2I/D=W_{el}$ into Eq. (21) gives

$$\tau_M = \left[1 + (n-1)\left(\frac{W_{el}}{M_y}(f_y + 0.002E) - 1\right)\left(\frac{M_{r1}}{M_y}\right)^{n-2}\right]^{-1} \quad (22)$$

Substituting $W_{el}\, f_y=M_y$ into Eq. (22), the τ_M formulation is given by

$$\tau_M = \left[1 + (n-1)\frac{0.002E}{f_y}\left(\frac{M_{r1}}{M_y}\right)^{n-2}\right]^{-1} \quad (23)$$

Eq. (23) can be written in terms of the ratio of M_{r1}/M_p as follows:

$$\tau_M = \left[1 + (n-1)\frac{0.002E}{f_y}\left(\frac{M_{r1}W_{pl}}{M_p\, w_{el}}\right)^{n-2}\right]^{-1} \quad (24)$$

τ_M determined by Eq.(24) is assumed to be applicable to the deformation range when $M_y<M_{r1}\leq M_p$. To evaluate the ability of τ_M to capture spread of plasticity through cross-section and along member length, simply supported beams (with a wide range of cross-sections and material properties) subjected to varied load cases are studied. τ_M determined by Eq.(24) are compared against flexural stiffness reduction derived from M-k curves of GMNIA. The derivation of flexural stiffness reduction is based on Eq. (18), where $dM_{r1}/d\kappa$ is the slope of the tangent at a given point on the M-k curve. The calculation of tangent slope is conducted through MATLAB 2017b [44].

Two examples, a beam with cross-section 200x100x10 (basic material parameters: E=175GPa, f_y=400MPa, n=6, W_{pl}/W_{el}=1.27, and M_p=140.8 kN*m) subjected to a pair of identical end moments, and a beam with cross-section 120x80x6 (E=190GPa, f_y=370MPa, n=7, W_{pl}/W_{el}=1.23, M_p=33.2 kN*m) subjected to uniform distributed load, are presented. For the two beams, the M-k curves determined by GMNIA are shown in Fig.8 (a) and (c). Comparison of τ_M derived from M-k

curves of GMNIA (denoted by $\tau_{M\text{-}GMNIA}$) and τ_M determined by equations (denoted by $\tau_{M\text{-}Eq}$) is shown in Fig.8 (b) and (d). It is observed that, τ_M determined by Eq. (24) is lower than τ_M determined by GMNIA. The discrepancy between $\tau_{M\text{-}Eq}$ and $\tau_{M\text{-}GMNIA}$ relies on the ability of the adopted moment-curvature relationship (based on Ramberg-Osgood curve) to capture accurately the moment-deflection behavior of the studied beams. Further analysis shows that, for the deformation range when $0 < M_{r1} \leq M_y$, replacing the term (n-1) by (n-1)/2 generates more accurate results. Thus, the modified τ_M formulation, given by Eq. (25), is adopted to predict flexural stiffness reduction before extreme fiber of the cross-section yields (Corresponding to M_y).

$$\tau_M = \left[1 + (n-1)\frac{0.002E}{2 \cdot f_y}\left(\frac{M_{r1} W_{pl}}{M_p\, w_{el}}\right)^{n-2}\right]^{-1} \quad (25)$$

After extreme fiber of the cross-section yielding, plastic strain may increase at a high rate, and results in rapid increase of plastic curvature (κ). For the deformation range when $M_y < M_{r1} \leq M_p$, the flexural stiffness reduction factor, given by Eq. (26) is proposed in this paper. The development of Eq. (26) is based on the moment-curvature relationship (determined by GMNIA) of beams with a wide range of cross-sections and material properties.

$$\tau_M = \left[\left(1 - \frac{M_{r1}}{M_p}\right)\frac{1}{1 - \frac{w_{el}}{W_{pl}}}\right]^{0.9}\left[1 + (n-1)\frac{0.002E}{2 \cdot f_y}\right]^{-1} \quad (26)$$

From Fig.8 (b) and (d), it is seen that $\tau_{M\text{-}Eq}$ determined Eq. (25) and (26) is in very close agreement with $\tau_{M\text{-}GMNIA}$, which shows that the adopted stiffness reduction formulations accurately captures spread of plasticity through cross-section and along member length.

5 Analytically determined beam-column flexural stiffness reduction factor

In this section, formulations that evaluate the maximum second order elastic moment ($M_{r2\text{-}E}$) within sway-restrained and sway-permitted beam-columns are first described. The analytical expression of τ_{MN} for beam-columns (elastic and inelastic) is then developed. The formulations that determine maximum second order elastic moments are assumed to be applicable to determine maximum second order inelastic moment ($M_{r2\text{-}P}$), if flexural stiffness reduction factor τ_{MN} is incorporated into the elastic critical buckling load. Lastly, the accuracy of GNA coupled with analytical τ_{MN} is verified for stainless steel beam-columns and structural sub-assemblages.

5.1 Maximum second order elastic moment within sway-restrained beam-columns

For elastic beam-columns with no relative lateral displacement between member ends (sway-restrained), the maximum second order elastic moment ($M_{r2\text{-}E}$) within the member can be calculated by amplifying maximum first order moment (M_{r1}), as shown in Eq.(27). The derivation of this equation is shown in Appendix A.

$$\frac{M_{r2-E}}{M_{r1}} \approx \frac{C_m}{1 - \frac{P_{r1}}{P_{e1}}} = B_{1-E} \geq 1 \quad (27)$$

$$P_{e1} = \frac{\pi^2 EI}{l^2} \quad (28)$$

The amplification factor $B_{1\text{-}E}$ evaluates P-δ the effects on maximum second order elastic moment ($M_{r2\text{-}E}$). $B_{1\text{-}E}$ has the same definition as the amplification factor B_1 provided in Appendix 8 of AISC 360-16 [3]. Equivalent uniform moment factor C_m accounts for the beneficial effects of moment gradient for beam-columns. The theoretical expression of C_m for sway-restrained beam-columns without transverse loadings is given by Eq. (A.4) in Appendix A. P_{e1} (K=1) is elastic critical buckling strength of the member with unbraced length. Since the theoretical expression of C_m is impracticable for engineering design, a simplified linear expression for C_m has been proposed by Austin [45], given by

$$C_m = 0.6\text{-}0.4(M_1/M_2) \quad (29)$$

where M_1 and M_2 are the applied external end moments, $|M_1| \leq |M_2|$.

For sway-restrained beam-columns with transverse loadings in this study, the Austin equation is adopted. It does not consider material non-linearity, however, according to the research findings of Chen (Chapter 2 of [46]), the derived C_m considering material non-linearity is always lower than the solutions of Austin equation, which means C_m determined by Eq.(29) is conservative and safe for design. For sway-restrained beam-columns with transverse loadings between member ends, C_m is determined by equation C-A-8-4 provided in Commentary on Appendix 8 of AISC 360-16 [3].

5.2 Maximum second order elastic moment within sway-permitted beam-columns

For sway-permitted elastic beam-columns, the maximum internal elastic moment (for a storey) within different columns caused by P-Δ effects and together with P-δ effects may be determined by amplifying maximum first order moment (M_{r1}) through the factor $B_{2\text{-}E}$, given by Eq.(30). It is essentially the expression of evaluating P-Δ effects provided in [47]. The amplification factor $B_{2\text{-}E}$ in this paper is based on a similar definition of factor B_2 provided in Appendix 8 of AISC 360-16 [3] for frames with lateral displacement between stories, where the influence of P-δ effects on the global behavior of the frame (including isolated beam-column) is considered indirectly through the factor R_M given by Eq. (32).

$$\frac{M_{r2-E}}{M_{r1}} \approx \frac{1}{1 - \frac{P_{story}}{R_M P_{e*-story}}} = B_{2-E} \geq 1 \quad (30)$$

$$P_{e*-story} = \frac{F_H h}{\Delta} \quad (31)$$

$$R_M = 1 - 0.15\frac{P_{mf}}{P_{story}} \quad (32)$$

where P_{story} is total vertical load transferred by the story ($P_{story} = \sum P_{r1}$); $P_{e^*\text{-story}}$ is elastic critical buckling (sway mode) strength of the story without R_M ($P_{e^*\text{-story}}$ in this paper is slightly different to $P_{e\text{-story}}$ provided in [3]); $P_{e^*\text{-story}}$ can be determined by side-sway buckling analysis or Eq.(31); F_H and Δ are first order total story shear force and relative story drift due to F_H, respectively; h is storey height; the factor R_M , accounts for P-δ effects on the overall response of the

structure, $0.85 \leq R_M \leq 1$; P_{mf} is total vertical load in columns of the story that are part of moment frames. For isolated sway-permitted elastic beam-column, $P_{e^*\text{-story}}$ is equal to P_{es}; $P_{es} = (\pi^{\wedge 2}\ EI)/(KL)^{\wedge 2}$; R_M=0.85.

It should be mentioned that $P_{e^*\text{-story}}/P_{story}$ corresponds to the definition of $\alpha_{cr,sw}$ provided in EN 1993-1-1:2015 (E) [7]; If R_M is taken as 1, $B_{2\text{-E}}$ then corresponds to second order sway effects factor K_{sw} provided in [7].

$$K_{sw} = \frac{1}{1 - \frac{1}{\alpha_{cr,\,sw}}} \tag{33}$$

5.3 Development of the analytical τ_{MN}

Analytical expressions of τ_{MN} for beam-columns are developed through extending the formulations (Eq.(27) and Eq.(30)) that evaluate second order effects for elastic beam-columns to inelastic range. These formulations are assumed to be applicable to determine maximum second order inelastic moment ($M_{r2\text{-P}}$) of beam-columns provided that flexural stiffness reduction factor τ_{MN} is incorporated into elastic critical buckling load.

For sway-restrained beam-columns including material non-linearity, through incorporating τ_{MN} into Eq.(27), it gives

$$\frac{M_{r2-P}}{M_{r1}} \approx \frac{C_m}{1 - \frac{P_{r1}}{P_{e-\tau MN}}} = B_{1-P} \geq 1 \tag{34}$$

where

$$P_{e-\tau MN} = \tau_{MN} P_{e1} = \frac{\pi^2(\tau_{MN} EI)}{l^2} \tag{35}$$

The amplification factor $B_{1\text{-P}}$ evaluates P-δ effects on maximum second order inelastic moment ($M_{r2\text{-P}}$).

Rewriting Eq.(34), the analytical solution of τ_{MN} can be expressed by

$$\tau_{MN} \approx \frac{P_{r1}}{(1 - C_m \frac{M_{r1}}{M_{r2-P}})(P_{e1})} \tag{36}$$

Similarly, for sway-permitted beam-columns including material non-linearity, through incorporating τ_{MN} into Eq.(30), it gives

$$\frac{M_{r2-P}}{M_{r1}} \approx \frac{1}{1 - \frac{P_{story}}{P_{e*-\,story-\tau MN}}} = B_{2-P} \geq 1 \tag{37}$$

where $P_{e*-\,story-\tau MN} = \tau_{MN} R_M P_{e*-\,story}$

(38)

In Eq.(37), the amplification factor $B_{2\text{-P}}$ evaluates P-Δ effects and together with P-δ effects on $M_{r2\text{-P}}$; $M_{r2\text{-P}}$ (for a storey) is the maximum internal second order moment within different columns in a storey.

Rewriting Eq.(37), τ_{MN} for sway-permitted inelastic beam-columns can be expressed by

$$\tau_{MN} \approx \frac{P_{story}}{(1 - \frac{M_{r1}}{M_{r2-P}})(R_M P_{e*-\,story})} \tag{39}$$

428 τ_{MN} determined by Eq.(36) and Eq.(39) accounts for the influence of member out-of-straightness, residual stresses and
429 spread of plasticity, provided that the maximum second order inelastic moment ($M_{r2\text{-}P}$) in these equations are obtained from
430 an analysis that includes corresponding out-of-straightness, residual stresses and material non-linearity.
431 Note that although an equivalent uniform moment factor C_m is explicitly used in Eq. (36) and C_m is implicitly included in
432 Eq.(39), Eq.(39) is essentially the same as Eq.(36). It should be stressed that, the concept of C_m is, by amplifying the
433 maximum first-order moment of pinned beam-column subjected to a pair of equal and opposite end moments, to obtain the
434 maximum total second order moment of beam-columns with different loading conditions (varied moment distribution along
435 member) and different boundary conditions, as illustrated in Appendix A. In Eq.(39), the influence of different loading
436 conditions (moment distribution) and different boundary conditions is implicitly included in the ratio of $P_{story}/P_{e*\text{-}story}$ (or
437 P_{r1}/P_{es}), where the accuracy of $P_{e*\text{-}story}$ (or P_{es}) depends on the column effective length (K) that amplifies the length of
438 pinned column.
439 It is worth noting that although second order moments caused by P-δ or P-Δ effects may have different distribution to first
440 order elastic moments (altering the location of maxima), one should keep in mind that member sizes are governed by the
441 value of the maximum moment rather than the location of the maximum moment in practical design.

442 **5.4 Verification of the analytical τ_{MN}**

443 The accuracy of GNA with the analytically determined τ_{MN} is verified in this section. A series of beam-columns including
444 simply supported beam-columns, cantilever beam-columns, and beam-columns in structural sub-assemblages, are studied.
445 All members bend about major axis (except the cases specified with minor axis bending).
446 The maximum second order moment within a member obtained from GMNIA and that obtained from GNA with τ_{MN} are
447 denoted by $M_{r2\text{-}GMNIA}$ and $M_{r2\text{-}\tau MN}$, respectively. The target of the verification study in this section is that $M_{r2\text{-}\tau MN}$ provided
448 by GNA with analytical τ_{MN}, should tend towards, or close to $M_{r2\text{-}GMNIA}$ provided by GMNIA.

449 **5.4.1 Steps for verification**

450 Verification study for sway-restrained beam-columns and sway-permitted beam-columns are carried out through the
451 following steps, as illustrated in Fig.9.

452 (1) Perform GMNIA analysis for beam-columns subjected to factored loading.
453 Out-of-straightness of 0.001 is introduced to simply supported beam-columns and sway-restrained sub-assemblages
454 while out-of-plumbness of 0.002 and out-of-straightness of 0.001 are introduced to cantilever beam-columns and
455 sway-permitted sub-assemblages. The maximum second order moment and axial force within a member determined
456 by GMNIA are denoted by $M_{r2\text{-}GMNIA}$ and $P_{r2\text{-}GMNIA}$, respectively.
457 (2) Perform Linear Elastic Analysis (LA)

The applied loads are same to those in GMNIA. P_{r1}, M_{r1}, C_m, P_{story} , $P_{e^*\text{-}story}$ and R_M are obtained.

(3) Calculate analytically determined τ_{MN}.

For sway-restrained and sway-permitted beam-columns that experience inelastic stage, τ_{MN} is calculated according to Eq. (36) and Eq. (39), respectively. In such calculation, $M_{r2\text{-}P}$ is taken as $M_{r2\text{-}GMNIA}$. Note that for beam-columns in elastic stage, analytical solution of τ_{MN} is equal to unity.

(4) Perform GNA with τ_{MN} analysis

Under the same load applied in GMNIA, GNA with τ_{MN} (denoted by GNA-τ_{MN}) is conducted. The maximum second order moment and axial force within a member obtained from GNA-τ_{MN} are denoted by $M_{r2\text{-}\tau MN}$ and $P_{r2\text{-}\tau MN}$, respectively. Out-of-straightness is not introduced in GNA-τ_{MN}, since the influence of out-of-straightness of 0.001 is intended to be included in the above τ_{MN}. Thus, when conducting GNA-τ_{MN}, only out-of-plumbness of 0.002 is considered for cantilever beam-columns and sway-permitted sub-assemblages, while no geometric imperfection is considered for sway-restrained beam-columns. The material stress-strain curve for GNA-τ_{MN} does not include the effect of residual stress, because the influence of residual stresses is included in τ_{MN}. $M_{r2\text{-}\tau MN}$ are verified against $M_{r2\text{-}GMNIA}$.

Note that $M_{r2\text{-}GMNIA}$ contains both maximum second order elastic moment and maximum second order inelastic moment. In the elastic range, $M_{r2\text{-}GMNIA}$ refers to $M_{r2\text{-}E}$ of the member and the analytical solution of τ_{MN} is actually equal to 1, since both internal axial force and moments are small. With P_{r1} and M_{r1} increasing, the beam-column reaches to inelastic range, and consequently $M_{r2\text{-}GMNIA}$ represents $M_{r2\text{-}P}$ of the member.

5.4.2 Verification study for simply supported beam-columns and cantilever beam-columns

Simply supported beam-columns (shown in Fig.10.) with cross-section 120x80x6 (basic material parameters: E=175GPa, f_y=350MPa, and n=7; λ_c=0.65) are first studied. The beam-columns are subjected to a combination of axial load (P) and moments (M_1, M_2) at the ends. P is a continuously factored load; M_2=e*P; "e" ranges from 5 to 150 (e= [5,10,20,30,50,100,150]) and the unit of e is mm; M_1=s*M_2; the non-dimensional factor s ranges from -1 to 1(s= [-1,-0.5,0, 0.5, 1]) ; $|M_2|\geq|M_1|$. For the simply supported beam-columns, one focus is whether the influence of non-uniform bending moments (moment gradient) on inelastic maximum second order moments is well captured by τ_{MN}. Non-uniform bending moments are produced by applying varied end moments. End moment variation is controlled by the non-dimensional factor s.

The normalized strength curves ($M_{u\text{-}GMNIA}/M_p$ versus $P_{u\text{-}GMNIA}/P_y$) provided by GMNIA are shown in Fig 10 (a), where $P_{u\text{-}GMNIA}$ is the ultimate axial load for a given factor *e* and *s*, and the corresponding ultimate external moment (denoted by $M_{u\text{-}GMNIA}$) is equal to M_2. By varying "s", it is observed that the benefit of moment gradient is considerable for the studied

beam-columns.

Comparison of $M_{r2\text{-}GMNIA}$ against $M_{r2\text{-}\tau MN}$ for the studied beam-columns is shown in Fig 10 (b). In this figure, $M_{r2\text{-}GMNIA}$ and $M_{r2\text{-}\tau MN}$ are normalized by the maximum first order internal bending moment M_{r1} obtained from Linear Elastic Analysis (LA). Similarly, the maximum second order internal axial force $P_{r2\text{-}GMNIA}$ and $P_{r2\text{-}\tau MN}$ are normalized by cross-section yield strength (P_y). It is observed that for the case of uniform bending (s= -1), $M_{r2\text{-}\tau MN}$ values are in very close agreement with $M_{r2\text{-}GMNIA}$. For the cases of non-uniform bending moment ($s \neq -1$), a slight discrepancy between $M_{r2\text{-}GMNIA}$ and $M_{r2\text{-}\tau MN}$ occurs in the inelastic range. For the studied simply supported beam-columns, it can be concluded that GAN coupled with τ_{MN} determined by Eq.(36) gives accurate predictions. It indicates the above-described assumption for sway-restrained beam-columns is sound, and the influence of moment gradient on the maximum second order inelastic moment is well captured by the analytical τ_{MN}.

Cantilever beam-columns (shown in Fig.11) with cross-section 100x100x5 (E=180 GPa, fy=370MPa, and n=6), subjected to a combination of axial (P) and transverse (0.1P) loads at the cantilever end, are then studied. The applied load P is discretely factored, where $P=i\cdot P_{u\text{-}GMNIA}$; i is less than 1 and it has 7 different values for each cantilever beam-column; $P_{u\text{-}GMNIA}$ is the ultimate axial load of a cantilever beam-column under the combined loading determined by GMNIA. The cantilever beam-columns have different column slenderness (λ_c): 0.73, 0.95, 1.1, 1.25, and 1.47.

Comparison of $M_{r2\text{-}GMNIA}$ and $M_{r2\text{-}\tau MN}$ is shown in Fig.11. $M_{r2\text{-}GMNIA}$ and $M_{r2\text{-}\tau MN}$ are normalized to M_{r1} and $P_{r2\text{-}GMNIA}$ and $P_{r2\text{-}GNA\text{-}\tau MN}$ are normalized by cross-section yield strength (P_y). Compared to P_y, the ultimate axial load of the studied cantilever beam-columns is relatively small, and consequently the ratio of P_{r2} to P_y is small, as observed. For cantilever beam-columns with varied column slenderness (λ_c), the maximum second moments obtained from GNA-τ_{MN} agree well with those obtained from GMNIA. As the applied axial load P increases, a slight discrepancy between $M_{r2\text{-}GMNIA}$ and $M_{r2\text{-}\tau MN}$ occurs in the inelastic range. For the studied cantilever beam-columns, it can be concluded that GAN with τ_{MN} determined by Eq.(39) gives accurate predictions. It demonstrates that the above assumption for sway-permitted beam-columns is reasonable and the analytically determined τ_{MN} is accurate.

Lastly, a series of simply supported and cantilever beam-columns with varied cross-sections and material properties, (shown in Table 2) are studied. 3 different column slenderness (λ_c), where $0.5 \leq \lambda_c \leq 1.5$, are considered for each cross-section. The loading cases are shown in Fig.12, where the applied axial load is factored load for all the cases, and the unit of the *e* is mm for the simply supported beam-columns. Some minor axis bending moment cases are studied for RHS beam-columns. The accuracy of GNA-τ_{MN} is assessed using the newly defined parameter ε. $\varepsilon = M_{r2\text{-}\tau MN} / M_{r2\text{-}GMNIA}$. The predicted results are shown in Table 2, where N_ε is the total number of ε for a particular group; ε_{av} and ε_{cov} indicate average values of ε and the coefficient of variation (COV). $\varepsilon+$ and $\varepsilon-$ are the maximum and minimum value of ε in the group.

Table 2. The studied beam-columns with varied cross-sections and basic material parameters, and the predicted results

Beam-column	Cross-section	Load case	Bending axis	E (GPa)	f_y (MPa)	n	W_{el}/W_{pl}	$\mathbf{N}_\varepsilon$	ε_{av}	ε_{cov}	ε+	ε-
Simply supported	80x80x4	SL	Major	200	300	6	0.85	105	0.99	0.008	1.03	0.97
	150x100x8		Major	175	350	8	0.85	105	1.01	0.010	1.03	0.96
	150x100x8		Minor	175	350	8	0.85	105	0.98	0.008	1.02	0.97
	160x80x8	SL-T	Major	190	450	5	0.84	48	0.97	0.017	1.07	0.93
	160x80x8		Minor	190	450	5	0.84	48	0.96	0.013	1.04	0.93
	150x150x8		Major	190	400	7	0.79	48	1.05	0.021	1.08	0.95
Cantilever	80x60x4	CL	Major	175	350	5	0.85	63	0.98	0.013	1.05	0.94
	80x60x4		Minor	175	350	5	0.85	63	1.04	0.022	1.05	0.93
	200x200x10		Major	175	450	9	0.82	63	1.03	0.010	1.06	0.95
	150x120x10		Major	190	400	6	0.82	63	0.99	0.019	1.05	0.94

It can be seen that, the COVs for the studied beam-columns are about 0.008-0.022, which indicates a small scatter of the ratio of $M_{r2\text{-}\tau MN}$ / $M_{r2\text{-}GMNIA}$. The ε_{av} for all the beam-columns are about 0.96 –1.05, which demonstrates that the maximum internal second order moment determined by GNA-τ_{MN} are in very close agreement with those determined by GMNIA. The maximum ε+ and ε- are 1.08 and 0.93, respectively. From the perspective of practical design, the maximum error of overestimation and underestimation of $M_{r2\text{-}GMNIA}$ are in acceptable range. GNA-τ_{MN} gives good results for both minor axis bending cases and major axis bending cases. This is because the proposed τ_{MN} does not rely on which axis the member bent about and GNA-τ_{MN} applies to both major and minor axis bending cases. From Table 2, it confirms again that GAN coupled with the analytically determined τ_{MN} gives accurate predictions and indicates that the above-described assumption for both sway-restrained and sway-permitted beam-columns is sound.

5.4.3 Verification study for beam-columns in structural sub-assemblages

Further verification study is conducted for beam-columns in structural sub-assemblages. The studied beam-columns present double curvature in sway-restrained sub-assemblages (C1, shown in Fig. 13 (a)), single curvature in sway-restrained sub-assemblages (C2, shown in Fig. 13 (b)), and double curvature in sway-permitted sub-assemblages (C3, shown in Fig. 13 (c)).

The details of cross-section and basic material parameters (additional material parameters are determined in terms with

basic parameters [27]) are shown in Table 3. Geometry and boundary conditions are shown in Fig. 13. Factored uniformly distributed loads (q) are applied on beams, concentrated loads (P) and bending moment (M) are applied on top and bottom of the columns, where P=qL; M=100mm*P; L is the length of the beam.

Table 3. Cross-sections and basic material parameters for the studied sub-assemblages

Sub-assemblage	Beam-column	Curvature	Cross-section	E (GPa)	f_y (Mpa)	n	W_{pl}/W_{el}
Sway-restrained (a)	C1	double	120x80x6	200	300	6	1.23
		double	120x80x6	200	350	6	1.23
Sway-restrained (b)	C2	single	200x100x10	190	350	7	1.27
		single	200x100x10	175	455	7	1.27
Sway-permitted (c)	C3	double	150x100x10	190	400	7	1.25
		double	150x100x10	200	450	7	1.25

Comparison of $M_{r2\text{-}GMNIA}$ against $M_{r2\text{-}\tau MN}$ for the studied beam-columns in structural sub-assemblages is shown in Fig.14. In this figure, the vertical axis represents selected load ratios (λ). $M_{r2\text{-}GMNIA}$ and $M_{r2\text{-}\tau MN}$ are normalized by M_{r1} (determined by LA). It is observed that for all the cases, the maximum second moments obtained from GNA-τ_{MN} is in close agreement with those obtained from GMNIA in both elastic and inelastic ranges. For beam-column C2, it seems that the discrepancy between $M_{r2\text{-}\tau MN}$ and $M_{r2\text{-}GMNIA}$ increases as the load ratio (λ) increases. However, it can be seen that the maximum error is within 5%. It can be concluded that GNA coupled with τ_{MN} determined by the above-described two analytical expressions provides accurate predictions for the studied beam-columns in structural sub-assemblages. It further demonstrates the extension of formulations for evaluating elastic second order effects to determine inelastic maximum second order moment is sound, provided that τ_{MN} is incorporated into elastic critical buckling load.

6. Approximately determined beam-column stiffness reduction factor

6.1 Development of the approximate τ_{MN}

Since the maximum second order internal moment ($M_{r2\text{-}P}$) is unknown in the actual design cases, the analytically determined τ_{MN} can not be applied directly. The aim of proposing the analytically determined τ_{MN} is to develop an approximate expression for τ_{MN} (has no relationship with $M_{r2\text{-}P}$) which can be applied in practice.

As flexural stiffness reduction factor of a carbon steel beam-column can be determined by a function that includes relevant variables without $M_{r2\text{-}P}$ [6, 13, 16-19], a function (approximate expression) independent of $M_{r2\text{-}P}$, which matches analytical expression of τ_{MN}, is proposed. The variables in the proposed approximate expression consist of P_{r1} , M_{r1}, C_m, W_{el}/W_{pl} (cross-section shape factor), $B_{2\text{-}E}$, τ_N (τ_N depends on P_{r1}), and τ_M (τ_M depends on M_{r1} and basic material parameters).

The approximate expression of τ_{MN} is developed by fitting variables to the analytical expressions determined by Eq.(36) and Eq.(39), as illustrated in Fig.15. The fitting process is carried out through running codes in MATLAB (2017b) [44]. Since member out-of-straightness of 0.001, residual stresses and spread of plasticity are take into consideration in the analytically determined τ_{MN}, these factors are consequently included in the approximately determined τ_{MN}.

The approximate expression of τ_{MN} is given by Eq.(40). It is based on the numerical study of stainless steel beam-columns with a wide range of cross-sections, length, material properties, and boundary conditions. Uncertainty in material strength and stiffness is not considered here, since it is intended to be accounted for through the resistance factor $\square_c$ and $\square_b$ in beam-column interaction design equations (shown in section 3).

$$\tau_{MN} = \gamma\Omega_M\tau_N\tau_M\left[1-\left(\frac{P_{r1}}{P_y}\right)^{0.9}\left(C_m\frac{M_{r1}}{M_p}\right)^{\frac{W_{el}}{W_{pl}}}\right] \quad (40)$$

$$0.8 \le \gamma = 2(B_{2-E} - 0.6) < 1 \quad \text{for } 1 \le B_{2\text{-}E} < 1.1 \quad (41)$$

$$\gamma = 1 \quad \text{for } 1.1 \le B_{2\text{-}E} \quad (42)$$

$$\Omega_M = 1 \quad \text{for } 0 \le \frac{M_{r1}}{M_p} < 0.4 \quad (43)$$

$$\Omega_M = \left(0.6 + \frac{M_{r1}}{M_p}\right)^{1.4} \quad \text{for } 0.4 \le \frac{M_{r1}}{M_p} \le 1 \quad (44)$$

It should be noted that, for sway-restrained beam-columns, the factor $B_{2\text{-}E}$ is taken as 1. The proposed equation is affected by $B_{2\text{-}E}$ factor ($B_{2\text{-}E} \ge 1$). $B_{2\text{-}E} < 1.1$ means the increase of internal forces and moments due to P-Δ effects and together with P-δ effects may be no more than 10%.

For the cases of $1 \le B_{2\text{-}E} < 1.1$, when M_{r1} and P_{r1} are close to 0, the upper bound for τ_{MN} would be $\gamma \cdot \tau_N$ and $\gamma \cdot \tau_M$, respectively. For the cases of $1.1 \le B_{2\text{-}E}$, when M_{r1} and P_{r1} are close to 0, the asymptotic upper bound of τ_{MN} is τ_N and τ_M, respectively. When $\gamma=1$ and $M_{r1}/M_p \le 0.4$, Eq.(40) has the similar formation to beam-column stiffness reduction expression proposed by Kucukler et.al [6, 16], Kucukler and Gardner [17-19].

A three-dimensional (3D) plot of τ_{MN} determined by Eq. (40) for beam-columns with two typical cross-sections is shown in Fig. 16. For the beam-column with cross-section 150x100x8 (basic material parameters: n=6, f_y=350MPa and E=200GPa), $B_{2\text{-}E}$ is assumed to be equal to 1.0 (sway-restrained, γ =0.8) and moment gradient factor C_m is assumed to be equal to 1.0 (subjected to a pair of equal but opposite end moments). For the beam-column with cross-section 150x150x10 (basic material parameters: n=7, f_y=450MPa and E=190GPa), $B_{2\text{-}E}$ is assumed to be larger than 1.1 (sway-permitted, γ =1) and C_m is assumed to be equal to 0.6 (subjected to only one end moment).

6.2 Verification of the approximate τ_{MN}

The accuracy of GNA with the approximately determined τ_{MN} (GNA-τ_{MN}) is verified for three statically indeterminate

frames. Moreover, the proposed method is compared against the direct analysis method (DM). In implementing DM, the reduced flexural stiffness $0.8\tau_N$ is adopted. The predicted results of GNA-τ_{MN} and DM are compared against those determined by GMNIA.

6.2.1 Geometries and loads of the studied stainless steel frames

Two-bay two-storey frames with pinned end and a two-bay five-storey frame with fixed end, are studied. All beam-to-column joints of the studied frames are rigid. The geometry of the studied frames are shown in Fig.17, where the frames shown in (a), (b), and (c) are referred to as Frame-2X2-G, Frame-2X2-GW and Frame-2X5-GW, respectively. Members of the two-bay two-storey frames have varied cross-sections, while all members of Frame-2X5-GW have the same cross-250x150x10. The use of the same cross-section for all members is intended to obtain widely dispersed flexural stiffness reduction factor τ_{MN}. All beams and columns for the studied frames bend about major axis. The details of design load combinations and basic material parameters (additional parameters are determined in terms with basic parameters [27]) are provided in Table. 4.

Table. 4 Details of the studied frames

Frame	Load combination	Cross-section	E(GPa)	f_y (MPa)	n
Frame-2X2-G	$1.2D_n+1.6L_n$	Varied	200	400	7
Frame-2X2-GW	$1.2D_n+0.5L_n+1.6W_n$	Varied	200	400	7
Frame-2X5-GW	$1.2D_n+0.5L_n+1.6W_n$	250x150x10	190	450	7

For the two-bay two-storey frames, two types of load combination provided in [48] are considered: (a) Gravity load combination $1.2D_n+1.6L_n$, in which D_n and L_n denote nominal dead (gravity) load and nominal live (gravity) load, respectively, and the typical nominal live-to-dead load ratio L_n/D_n= 1.5. (b) Combination of wind load and gravity load $1.2D_n+0.5L_n+1.6W_n$, in which W_n denotes nominal wind load; live-to-dead load ratio L_n/D_n= 1.0, and wind-to-gravity load ratio $W_n/(L_n+D_n)$=0.1. For the 2x5 frame, one load case (wind load and gravity load $1.2D_n+0.5L_n+1.6W_n$) is considered. For all the frames, the combined load applied on the top-storey is half of that applied on other storeys.

6.2.2 Procedure of implementing GNA-τ_{MN}, GNA-τ_N and GMNIA

The procedure of implementing GNA-τ_{MN}, DM and GMNIA, involves the following steps:

(1) Define the design load

Given an assumed factored load, a GMNIA analysis is conducted. The applied load is defined as a design load when the Demand-Capacity ratio (R_c) of the critical member is equal to 1.0.

(2) Perform Linear Elastic Analysis (LA)

A Linear Elastic Analysis (LA) under the design load is conducted to obtain P_{r1}, M_{r1}, P_{story}, and $P_{e^*\text{-story}}$. Then τ_N, τ_M, C_m, R_M, and $B_{2\text{-}E}$ are calculated according to related equations. The flexural stiffness reduction factor τ_{MN} determined by Eq.(40)

is subsequently calculated.

(3) Perform GNA-τ_{MN} and DM

Under the design load, GNA-τ_{MN} and DM are conducted to obtain the maximum internal second order forces and moments, and Demand-Capacity ratios of the members. In implementing DM, the reduced flexural stiffness $0.8\tau_N$ is adopted.

In the implementation of GMNIA, out-of-plumbness of 0.002 and out-of-straightnes of 0.001 are introduced, and residual stress is considered through modified stress-strain curves. For GNA-τ_{MN} and DM, since the influence of out-of-straightness of 0.001 and residual stresses are included in the flexural stiffness reduction factor (τ_{MN} for GNA-τ_{MN}; $0.8\tau_N$ for DM), only out-of-plumbness of 0.002 is introduced to the frame models.

6.2.3 Comparison of predicted results. 2X2-G and 2X2-GW

For the studied two-bay two-storey frames, since the ratio of axial force to cross-section yield strength of all the members is very small, the Demand-Capacity ratio (R_c) of these members is very close to the ratio of maximum second moment to plastic moment (M_{r2}/M_P). Comparison of the predicted results from different methods is focused on the ratio of $R_{c\text{-}\tau MN}$ /$R_{c\text{-}GMNIA}$ and $R_{c\text{-}\tau N}$ /$R_{c\text{-}GMNIA}$, where $R_{c\text{-}GMNIA}$, $R_{c\text{-}\tau MN}$ and $R_{c\text{-}\tau N}$ represent R_c determined by GMNIA, GNA-τ_{MN} and DM, respectively, as shown in Table. 5. μ represents mean value and COV represents coefficient of variation.

Table. 5: Predicted results for the two-bay two-storey frames

Member	Frame-2X2-G					Frame-2X2-GW				
	GMNIA	**GNA-τ_{MN}**		**DM**		**GMNIA**	**GNA-τ_{MN}**		**DM**	
	$R_{c\text{-}GMNIA}$	τ_{MN}	$R_{c\text{-}\tau MN}$ / $R_{c\text{-}GMNIA}$	$0.8\tau_N$	$R_{c\text{-}\tau N}$ / $R_{c\text{-}GMNIA}$	$R_{c\text{-}GMNIA}$	τ_{MN}	$R_{c\text{-}\tau MN}$ / $R_{c\text{-}GMNIA}$	$0.8\tau_N$	$R_{c\text{-}\tau N}$ / $R_{c\text{-}GMNIA}$
C11	0.24	0.81	1.11	0.80	1.03	0.88	0.72	1.05	0.80	0.99
C12	0.42	0.79	1.04	0.80	0.82	0.87	0.76	1.16	0.80	1.00
C13	0.27	0.72	1.18	0.80	0.89	0.90	0.68	0.99	0.80	1.03
B11	0.33	0.79	0.98	0.80	1.02	0.96	0.76	1.12	0.80	0.96
B12	0.87	0.76	1.07	0.80	0.97	1.00	0.64	1.04	0.80	0.99
C21	0.49	0.84	1.09	0.80	1.03	0.32	0.90	1.00	0.80	0.93
C22	0.68	0.77	1.16	0.80	0.99	0.16	0.90	0.99	0.80	0.86
C23	0.96	0.67	0.96	0.80	0.93	0.78	0.67	1.00	0.80	1.02
B21	0.50	0.7	1.09	0.80	1.01	0.64	0.69	1.12	0.80	0.99
B22	1.00	0.66	1.06	0.80	0.96	0.67	0.63	1.00	0.80	1.02
μ			1.07		0.97			1.05		0.98
COV			0.07		0.06			0.06		0.05
Max			1.18		1.03			1.16		1.03
Min			0.96		0.82			0.99		0.86

In Table 5, the value of τ_{MN} (determined by the approximate expression) for different members is mainly dominated by the ratio of maximum first order moment to plastic moment (M_{r1}/M_P) and τ_M, since the ratio of axial force to cross-section

yield strength of all the members is very small (τ_N =1) . For all members, the value of 0.8τ_N is equal to 0.8. The critical members of both frames are beams whose failure is governed by the formation of first-plastic hinge (no elastic global buckling occurs in advance).

It is observed that $R_{c\text{-}\tau MN}$ is in close agreement with $R_{c\text{-}GMNIA}$ for the two frames, while $R_{c\text{-}\tau N}$ underestimates $R_{c\text{-}GMNIA}$ for most members, which means that DM provides unsafe predictions for these members. It should be pointed out that, under the same design load, safe prediction and unsafe prediction refer to overestimating $R_{c\text{-}GMNIA}$ and underestimating $R_{c\text{-}GMNIA}$, respectively. If $R_{c\text{-}\tau MN}$ ($R_{c\text{-}\tau N}$) is larger than $R_{c\text{-}GMNIA}$, it means that the predicted internal moments or axial forces are overestimated compared against those predicted by GMNIA. For the critical members (B22 of Frame-2X2-G and B12 of Frame-2X2-GW), GNA-τ_{MN} gives accurate and safe predictions, while DM underestimates $R_{c\text{-}GMNIA}$ of the critical members to some extent (within 5%).

The difference in the predicted results may be explained as follows. Firstly, τ_{MN} can more accurately capture stiffness reduction caused by spread of plasticity through cross-sections and along members. The accurate stiffness reduction for different members leads to reasonable distribution of internal force and moment. Secondly, since the two frames are very sensitive to second order effects, where the maximum value of $B_{2\text{-}E}$ is 1.60 and 1.41 for Frame-2X2-G and Frame-2X2-GW, respectively, the increase of internal forces and moments resulted from additional second order effects (due to material nonlinearity) are considerable. For GNA-τ_{MN}, the influence of additional second order effects due to material nonlinearity is well captured by the flexural stiffness reduction factor τ_{MN}. From Table 5, τ_{MN} is smaller than 0.8τ_N for most members and τ_{MN} for different members is not widely dispersed. It indicates that, for the two frames that are very sensitive to second order effects, a reduced flexural stiffness factor smaller than 0.8τ_N should be adopted when using DM.

6.2.4 Comparison of predicted results. 2X5-GW

Predicted results for Frame-2X5-GW are shown in Fig. 18. In this figure, the horizontal axis represents specific member in the frame (for example, 1 correspondents to C11, and 25 correspondents to B52); P_{r2}, M_{r2} and R_c determined by GNA-τ_{MN} and DM are compared against those determined by GMNIA. P_{r2} determined by GMNIA, GNA-τ_{MN} and GNA-τ_N, are denoted by $P_{r2\text{-}GMNIA}$, $P_{r2\text{-}\tau MN}$ and $P_{r2\text{-}\tau N,}$ respectively. For this frame, the maximum value of $B_{2\text{-}E}$ is 1.32, and the critical member is C12.

It is observed that, from the 3rd storey up to the top storey, the distribution of $R_{c\text{-}}\tau_{MN}/ R_{c\text{-}GMNIA}$ (or $R_{c\text{-}}\tau_N/ R_{c\text{-}GMNIA}$) is in very close agreement with the distribution of $M_{r2\text{-}}\tau_{MN}/ M_{r2\text{-}GMNIA}$ (or $M_{r2\text{-}}\tau_N/ M_{r2\text{-}GMNIA}$). This is because the ratio of axial force to cross-section yield strength is small for the columns in these storeys, and thus R_c is dominated by M_{r2}.

It is observed that, compared to DM, the predicted results of GNA-τ_{MN} have lower deviation from the predicted results of GMNIA. It indicates that GNA-τ_{MN} provides improved estimation for the studied frame. This is because τ_{MN} (determined

669 by the analytical expression) can more accurately capture stiffness reduction owing to material non-linearity, and well
670 capture additional second order effects due to material non-linearity. For the critical member (C12), both GNA-τ_{MN} and
671 DM provide accurate and safe predictions. Nevertheless, DM produces large errors for a few of other members. The
672 maximum error of overestimation of $R_{c\text{-}GMNIA}$ is within 13% for GNA-τ_{MN} and 20% for DM.
673 It is found that, for most members, the value of $M_{r2}\text{-}\tau_{MN}$/ $M_{r2\text{-}GMNIA}$ and $R_{c}\text{-}\tau_{MN}$/ $R_{c\text{-}GMNIA}$ is larger than 1. This may be
674 explained that τ_{MN} determined by the approximate expression is conservative. The conservative stiffness reduction
675 produces more deformations, which in turn results in increased second order effects (P-Δ and P-δ) and subsequently
676 increased internal bending moment and Demand-capacity ratio.
677 In addition, it should be mentioned that all the studied frames have not significant capacity for load redistribution. The
678 proposed approach may be very conservative for frames that significantly benefit from load redistribution and strain
679 hardening after the formation of the first plastic hinge. Furthermore, the applicability of the proposed approach for large
680 redundant structural systems that have complex interactions between members should be assessed.

681 **Conclusion**

682 In this paper, the flexural stiffness reduction factor for applying Geometrically Non-linear Analysis (GNA) to in-plane
683 stability design of stainless steel elements and multi-storey regular frames is proposed through analytical and numerical
684 study. The proposed beam-column flexural stiffness reduction factor (τ_{MN}) accounts for deleterious influence of spread of
685 plasticity, residual stresses and member out-of-straightness of 0.001. Two main aspects of developing τ_{MN} are: (1) Develop
686 the analytical expression of τ_{MN} through extending formulations that evaluate second order effects of beam-columns. These
687 formulations are extended to determine maximum second order inelastic moment of beam-columns by incorporating τ_{MN}
688 into elastic critical buckling load. (2) Develop the approximate expression of τ_{MN} (more likely to be used relative to the
689 analytical τ_{MN} in practice) by fitting relevant variables to the analytically determined τ_{MN} based on the results of numerical
690 study.
691 The accuracy of τ_{MN} determined by analytical expression are verified through comparison of the maximum bending
692 moments within members determined by GNA coupled with analytical τ_{MN} against those obtained from GMNIA. It is
693 observed that predicted results from GNA with analytical τ_{MN} are in very close agreement with those provided by GMNIA.
694 The accuracy of τ_{MN} determined by approximate expression is verified for frames with different geometrical and loading
695 configurations. It is found that, the predicted results from GNA coupled with the approximate τ_{MN} are in close agreement
696 with those provided by GMNIA. Compared to the Direct Analysis Method (DM), the proposed approach provides improved
697 estimations. One reason is the proposed τ_{MN} can more accurately capture stiffness reduction resulted from material non-
698 linearity and well capture additional second order effects due to material non-linearity.

Acknowledgement

The authors acknowledge the financial support provided by the Project BIA2016-75678-R, AEI/FEDER, UE "Comportamiento estructural de pórticos de acero inoxidable. Seguridad frente a acciones accidentales de sismo y fuego", funded from the MINECO (Spain). The authors acknowledge financial support from China Scholarship Council.

Appendix A

Maximum moment within an elastic beam-column is derived from differential equations governing the in-plane behavior of the member. Differential equations can be found in Chapter 2 of [39].

Maximum moment within an elastic beam-column subjected to varied end moments (shown in Fig. A.1 (a)) is determined by

$$M_{max} = M_2\left[\frac{\sqrt{\left(M_1/M_2\right)^2 + 2\left(M_1/M_2\right)coskl + 1}}{sinkl}\right] \quad \text{(A.1)}$$

where $= \sqrt{\frac{P}{EI}}$; $|M_2| \geq |M_1|$; l is the length of the beam-column.

Maximum moment within an elastic beam-column subjected to a pair of equal and opposite end moments (shown in Fig. A.1 (b)) is determined by

$$M_{max} = M_{eq}\left[\frac{\sqrt{2(1-coskl)}}{sinkl}\right] \quad \text{(A.2)}$$

Setting Eq. (A.2) equal to Eq. (A.1), it gives

$$M_{eq} = M_2\left[\frac{\sqrt{\left(M_1/M_2\right)^2 + 2\left(M_1/M_2\right)coskl + 1}}{2(1-coskl)}\right] \quad \text{(A.3)}$$

The expression in brackets is regarded as equivalent uniform moment factor (C_m)

$$\frac{\sqrt{\left(M_1/M_2\right)^2 + 2\left(M_1/M_2\right)coskl + 1}}{2(1-coskl)} = C_m \quad \text{(A.4)}$$

$$M_{eq} = M_2 C_m \quad \text{(A.5)}$$

Substituting Eq. (A.5) back into Eq. (A.2), it gives

$$M_{max} = M_2 C_m\left[\frac{\sqrt{2(1-coskl)}}{sinkl}\right] \quad \text{(A.6)}$$

Substituting $k = \sqrt{\frac{P}{EI}}$ back into the expression in brackets, it gives

$$\frac{\sqrt{2(1-coskl)}}{sinkl} = \frac{\sqrt{2\left(1-cos\left(\pi\sqrt{P/P_e}\right)\right)}}{sin\left(\pi\sqrt{P/P_e}\right)} = \sec\left(\frac{\pi}{2}\sqrt{P/P_e}\right) \approx \frac{1}{1-\frac{P}{P_e}} \quad \text{(A.7)}$$

723 Therefore, Eq. (A.6) can be approximately expressed by

724 $$\frac{M_{max}}{M_2} \approx \frac{C_m}{1-\frac{P}{P_e}} \quad \text{(A.8)}$$

725 Note that M_{max} , M_2, and P respectively correspondents to $M_{r2\text{-}E}$, M_{r1} and P_{r1} in section 5.1.

726 **References**

727 [1] ANSI/AISC 360-05, Specification for Structural Steel Buildings, American Institute of Steel Construction, Chicago,
728 2005.

729 [2] ANSI/AISC 360-10, Specification for Structural Steel Buildings, American Institute of Steel Construction, Chicago,
730 2010.

731 [3] ANSI/AISC 360-16, Specification for Structural Steel Buildings, American Institute of Steel Construction, Chicago,
732 2016.

733 [4] L.G. Griffis, D.W. White, Design Guide 28: Stability Design of Steel Buildings, American Institute of Steel
734 Construction, Chicago, 2013.

735 [5] D.W. White, A.E. Surovek, B.N. Alemdar et al., Stability analysis and design of steel building frames using the 2005
736 AISC Specification, Steel Structures 6 (2006) 71-91.

737 [6] M. Kucukler, L. Gardner, L. Macorini, Development and assessment of a practical stiffness reduction method for the
738 in-plane design of steel frames, Journal of Constructional Steel Research, 126 (2016) 187–200.
739 ***https://doi.org/10.1016/j.jcsr.2016.06.002***

740 [7] EN 1993-1-1(E) Final Draft: Eurocode 3: Design of steel structures - Part 1-1: General rules and rules for buildings,
741 Brussels, Belgium, 2017.

742 [8] EN 1993-1-1: Eurocode 3: Design of steel structures - Part 1-1: General rules and rules for buildings, Brussels,
743 Belgium, 2005. ***https://doi.org/10.3403/03270565***

744 [9] N. Baddoo, Design Guide 27: Structural Stainless Steel, American Institute of Steel Construction, Chicago, 2013.

745 [10] N. Baddoo, P. Francis, Development of design rules in the AISC Design Guide for structural stainless steel, Thin-
746 Walled Structures, 83 (2014) 200-208. ***https://doi.org/10.1016/j.tws.2014.02.007***

747 [11] ANSI/AISC 303-16, Code of standard practice for steel buildings, American Institute of Steel Construction, Chicago,
748 2016.

749 [12] B.G. Johnston, Guide to design criteria for metal compression members. 2nd. John Wiley & Sons, New York, 1966.

750 [13] D.W. White, W.Y. Jeong, O. Toga, Comprehensive stability design of planar steel members and framing systems via
751 inelastic buckling analysis, International Journal of Steel Structures 16(4) (2016)1029-1042.
752 ***http://dx.doi.org/10.1007/s13296-016-0070-3***

753 [14] A.E. Surovek-Maleck, D.W. White. Alternative approaches for elastic analysis and design of steel frames. I: Overview.
754 Journal of Structural Engineering ASCE 130(8) (2004)1186–96.
755 ***http://dx.doi.org/10.1061/(ASCE)0733-9445(2004)130:8(1186)***
756 [15] A.E. Surovek-Maleck, D.W. White. Alternative approaches for elastic analysis and design of steel frames. II:
757 Verification studies. Journal of Structural Engineering ASCE 130 (8) (2004) 1197–205.
758 ***http://dx.doi.org/ 10.1061/(ASCE)0733-9445(2004)130:8(1197)***
759 [16] M. Kucukler, L. Gardner, L. Macorini, A stiffness reduction method for the in-plane design of structural steel elements.
760 Engineering Structures 73 (2014) 72–84. ***https://doi.org/10.1016/j.engstruct.2014.05.001***
761 [17] M. Kucukler, L. Gardner, Design of hot-finished tubular steel members using a stiffness reduction method. Journal of
762 Constructional Steel Research.160 (2019), 340-358. ***https://doi.org/10.1016/j.jcsr.2019.05.039***
763 [18] M. Kucukler, L. Gardner, Design of laterally restrained web-tapered steel structures through a stiffness reduction
764 method. Journal of Constructional Steel Research. 141 (2018), 63-76. ***https://doi.org/10.1016/j.jcsr.2017.11.014***
765 [19] M. Kucukler, L. Gardner, Design of web-tapered steel beams against lateral-torsional buckling through a stiffness
766 reduction method. Engineering Structures. 190 (2019), 246-261. ***https://doi.org/10.1016/j.engstruct.2019.04.008***
767 [20] A.H. Zubydan. A simplified model for inelastic second order analysis of planar frames. Engineering Structures
768 32(10)(2010) 3258–68. ***https://doi.org/10.1016/j.engstruct.2010.06.015***
769 [21] ECCS. Ultimate limit state calculation of sway frames with rigid joints. Technical Committee 8 of European
770 Convention for Constructional Steelwork (ECCS), No 33, 1984.
771 [22] S.E. Kim, W.F. Chen, Design guide for steel frames using advanced analysis program, Engineering Structures 21
772 (1999) 352–364. ***https://doi.org/10.1016/S0141-0296(97)00209-5***
773 [23] Abaqus v.6.13 Reference Manual. Simulia, Dassault Systemes, 2013.
774 [24] E. Suli, D. Mayers, An introduction to numerical analysis, Cambridge University Press, Cambridge, 2003.
775 [25] Y.F. Shen, R. Chacon, Effect of uncertainty in localized imperfection on the ultimate compressive strength of cold-
776 formed stainless steel hollow sections, Applied Sciences. 9(18) (2019), 3827. ***https://doi.org/10.3390/app9183827***
777 [26] EN 1993-1-4: Eurocode 3: Design of steel structures - Part 1.4: General rules -Supplementary rules for stainless steel,
778 Brussels, Belgium, 2015. ***https://doi.org/10.3403/30126870***
779 [27] K.J.R. Rasmussen, Full-range stress–strain curves for stainless steel alloys, Journal of Constructional Steel Research.
780 59 (2003) 47–61. ***https://doi.org/10.1016/S0143-974X(02)00018-4***
781 [28] SEI/ASCE 8-02: Specification for the design of cold-formed stainless steel structural members, American Society of
782 Civil Engineers (ASCE), 2002. ***https://doi.org/10.1061/9780784405567***

783 [29] AS/NZS 4673: Cold-formed stainless steel structures, Standards Australia/Standards New Zealand, 2001.
784 [30] P. Hradil, A. Talja, Investigating the role of gradual yielding in stainless steel columns and beams by virtual testing,
785 in : Proceedings of the 5th International Conference on Structural Engineering, Mechanics and Computation (SEMC
786 2013). Cape Town, South Africa, 2013, 1459-1464.
787 [31] I. Arrayago, New approach for efficient design of stainless steel RHS and SHS elements, Doctoral thesis. Universitat
788 Politècnica de Catalunya, Barcelona, 2016.
789 [32] L. Gardner, D.A. Nethercot, Experiments on stainless steel hollow sections-Part 1: Material and cross-sectional
790 behavior, Journal of Constructional Steel Research. 60 (2004) 1291-1318. ***https://doi.org/10.1016/j.jcsr.2003.11.006***
791 [33] S. Afshan, B. Rossi, L. Gardner, Strength enhancements in cold-formed structural sections -Part 1: Material testing,
792 Journal of Constructional Steel Research. 83 (2013) 177–188. ***https://doi.org/10.1016/j.jcsr.2012.12.008***
793 [34] P.W. Key, G.J. Hancock, A Theoretical investigation of the column behavior of cold-formed square hollow sections,
794 Thin-Walled structures, 16(1993), 31-64. ***https://doi.org/10.1016/0263-8231(93)90040-H***
795 [35] L. Gardner, R. B. Cruise, Modeling of residual stresses in structural stainless steel sections, Journal of Structural
796 Engineering ASCE, 135(1)(2009) 42-53. ***10.1061/(ASCE)0733-9445(2009)135:1(42)***
797 [36] M. Jandera, L. Gardner, J. Machacek, Residual stresses in cold-rolled stainless steel hollow sections, Journal of
798 Constructional Steel Research 64 (2008) 1255–1263. ***https://doi.org/10.1016/j.jcsr.2008.07.022***
799 [37] R.B. Cruise, L. Gardner, Residual stress analysis of structural stainless steel sections, Journal of Constructional Steel
800 Research 64 (2008) 352–366. ***https://doi.org/10.1016/j.jcsr.2007.08.001***
801 [38] M. Jandera, J.Machacek, Residual Stress Influence on material properties and column behavior of stainless steel SHS,
802 Thin-Walled Structures 83(2014)12–18. ***https://doi.org/10.1016/j.tws.2014.03.013***
803 [39] W.Y. Liu, K. J.R. Rasmussen, H. Zhang, Modelling and probabilistic study of the residual stress of cold-formed
804 hollow steel sections, Engineering Structures 150 (2017) 986–995. ***https://doi.org/10.1016/j.engstruct.2017.08.004***
805 [40] R. D. Ziemian, Guide to stability design criteria for metal structures, Engineering and Technology Publishing, 2010.
806 ***http://dx.doi.org/10.1002/9780470549087***
807 [41] I. Arrayago, E. Real, E. Mirambell, Experimental study on ferritic stainless steel RHS and SHS beam-columns, Thin-
808 Walled Structures. 100 (2016) 93–104. ***https://doi.org/10.1016/j.tws.2015.12.004***
809 [42] W.F. Chen, Design of beam-columns in steel frames in the United States, Thin-Walled Structures 13(1–2) (1992) 1-
810 83. ***https://doi.org/10.1016/0263-8231(92)90003-F***
811 [43] E. Real, E. Mirambell, Flexural behaviour of stainless steel beams, Engineering Structures 27 (2005) 1465–1475.
812 ***https://doi.org/10.1016/j.engstruct.2005.04.008***

[44] Matlab 2017(b) Reference Manual. The MathWorks, 2019.

[45] W.J. Austin, Strength and design of metal beam-columns, Journal of the Structural Division, ASCE, 87(1961) 1–32.

[46] W.F. Chen, E.M. Lui, Stability design of steel frames, CRC Press, 2017. ***https://doi.org/10.1201/9781351076852***

[47] F. Cheong-Siat-Moy, Consideration of secondary effects in frame design, Journal of the Structural Division, ASCE, 103(10) (1977) 2005-19.

[48] ASCE/SEI 7-16, Minimum Design Loads and Associated Criteria for Buildings and Other Structures, American Society of Civil Engineers, Reston, 2016.

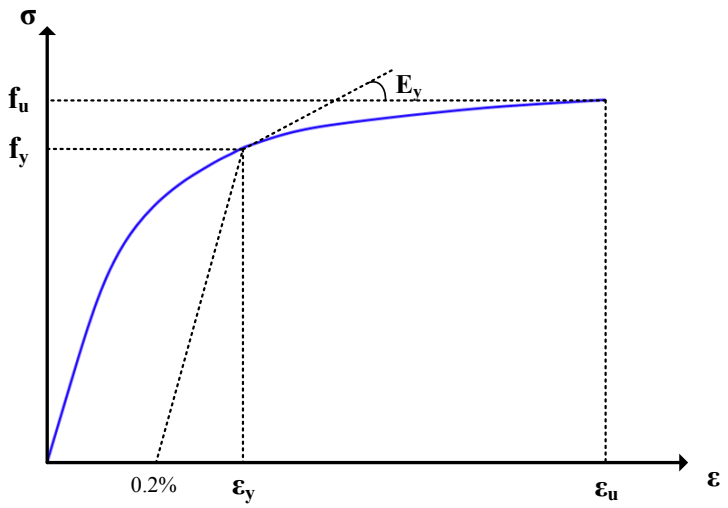

Fig.1. Adopted stress-strain curve for stainless steel

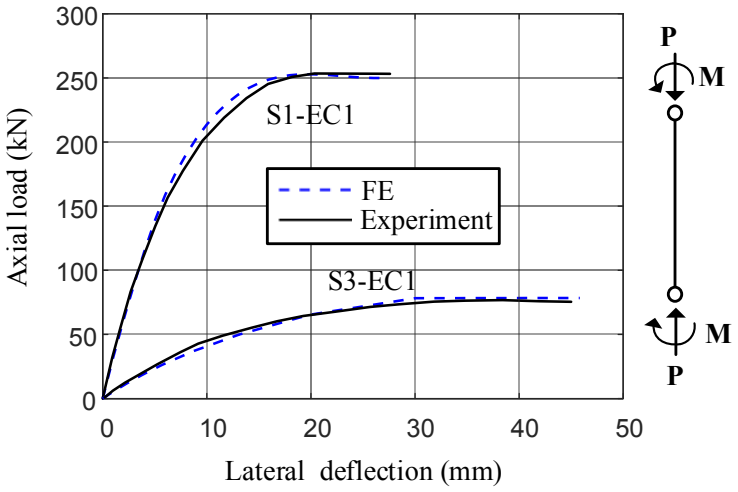

Fig.2. Validation of the developed FE models against experimental results reported in [41]

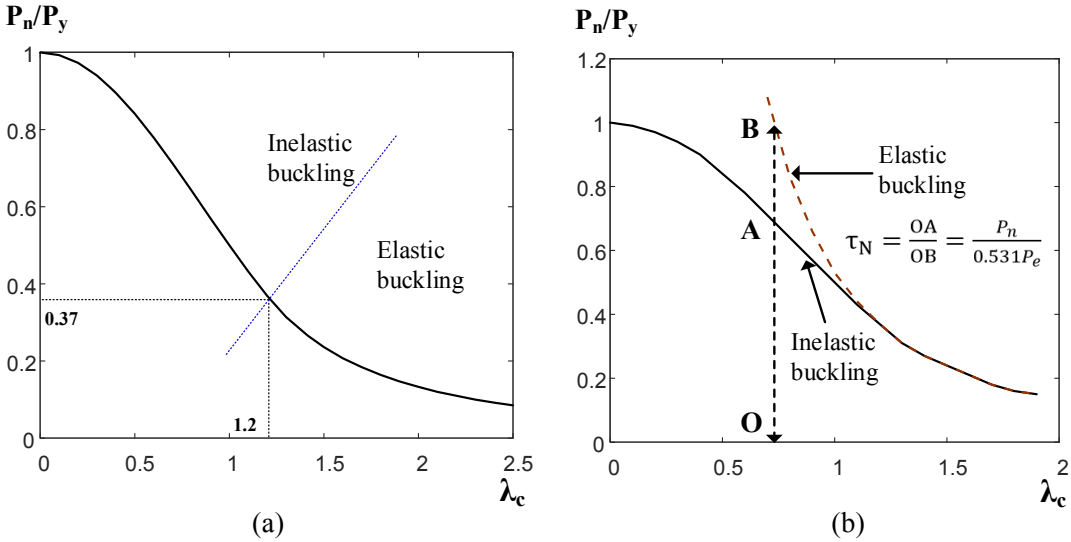

Fig.3. Column flexural buckling curve and illustration of the derivation of τ_N (a) AISC LRFD-based stainless steel column flexural buckling curve (b) Illustration of the derivation of the column stiffness reduction factor τ_N

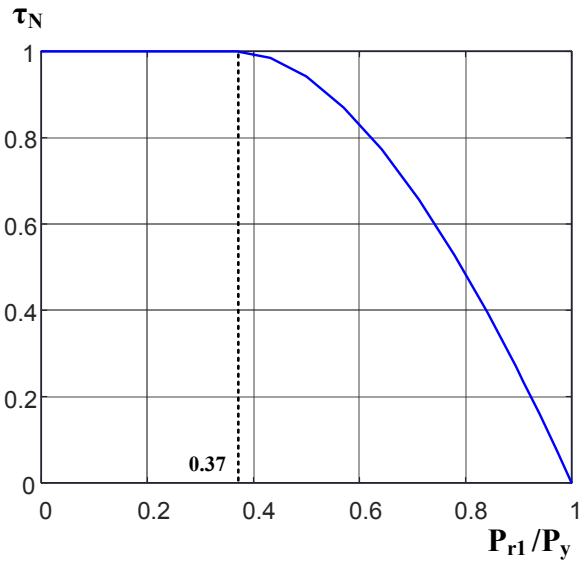

Fig.4 Flexural stiffness reduction factor (τ_N) for stainless steel column

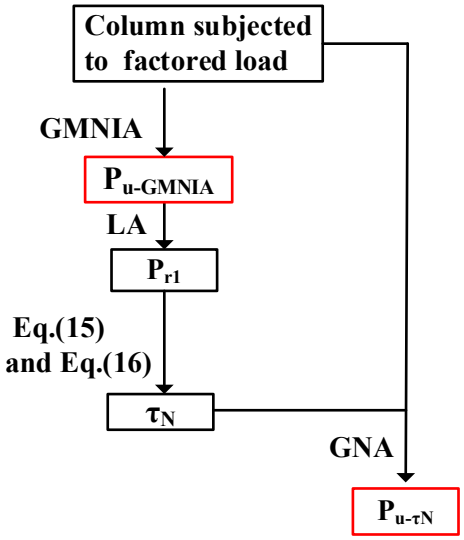

Fig.5. Verification procedure for the studied columns

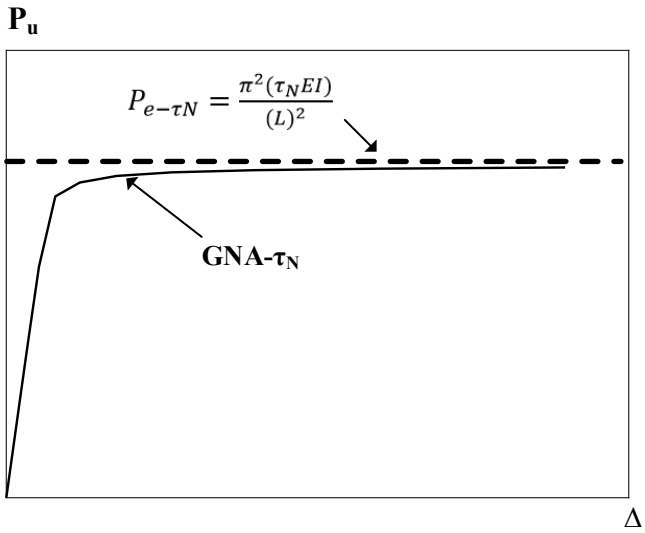

Fig.6. Comparison of the ultimate axial load (P_u) determined by GNA-τ_N against the elastic critical buckling load ($P_{e\text{-}\tau N}$) determined by the reduced flexural stiffness ($\tau_N EI$)

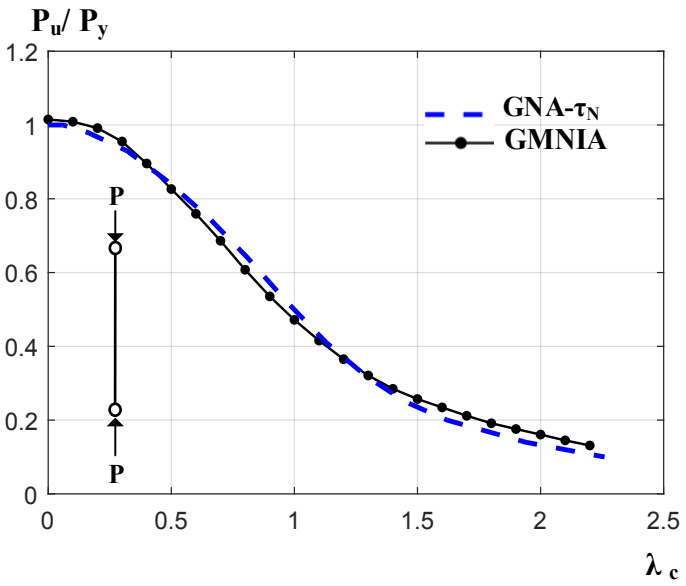

Fig.7. Normalized ultimate axial load (P_u/P_y) determined by different methods against column slenderness (λ_c)

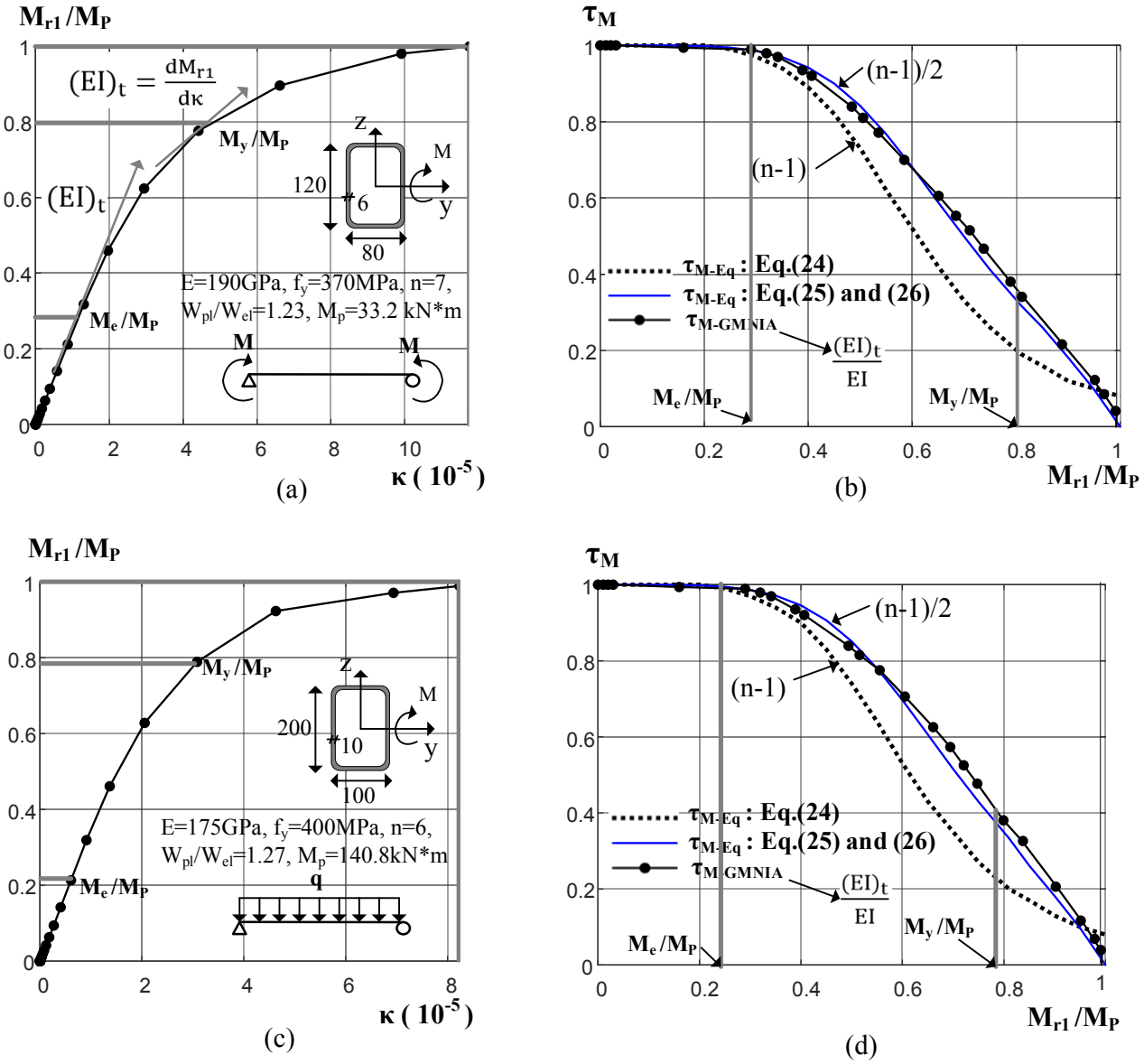

Fig.8 Evaluation of the flexural stiffness reduction factor (τ_M) for the studied stainless steel beams: (a) and (c): moment-curvature relationship determined by GMNIA. (b) and (d): comparison of τ_M determined by different methods

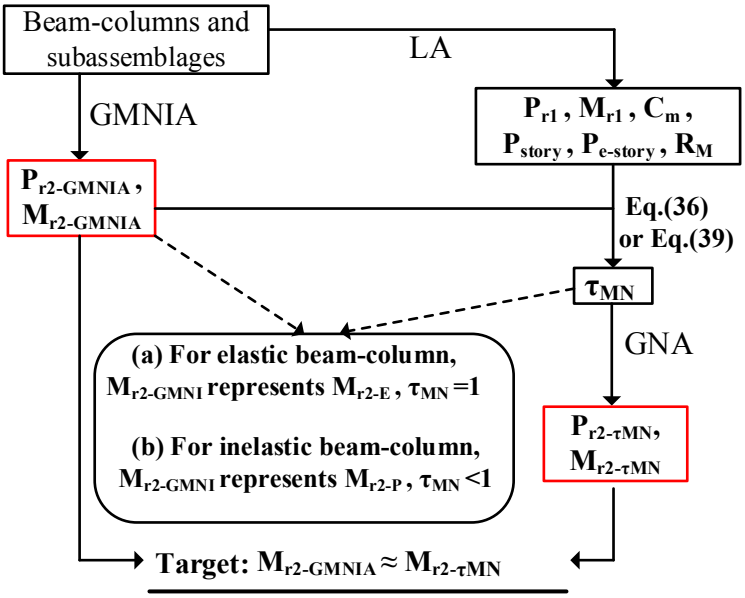

Fig.9 Procedure of conducting verification study for beam-columns and sub-assemblages

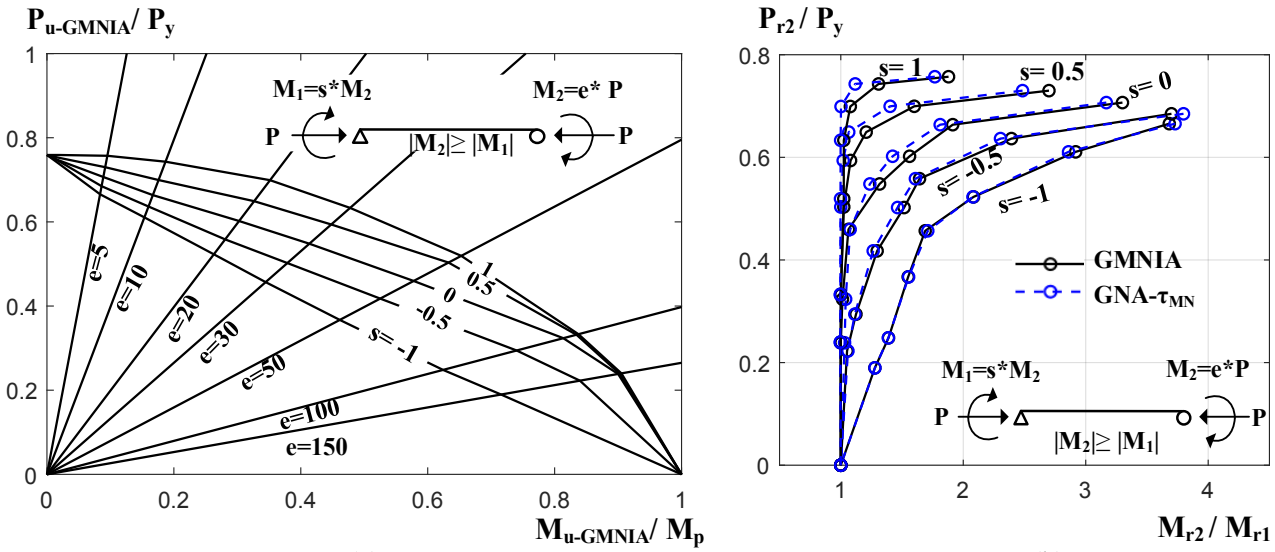

Fig.10 Predicted results for the simply supported stainless steel beam-columns (a) Strength curve under moment gradient determined by GMNIA, (b) Comparison of M_{r2} predicted by GMNIA against those determined by GNA-τ_{MN}

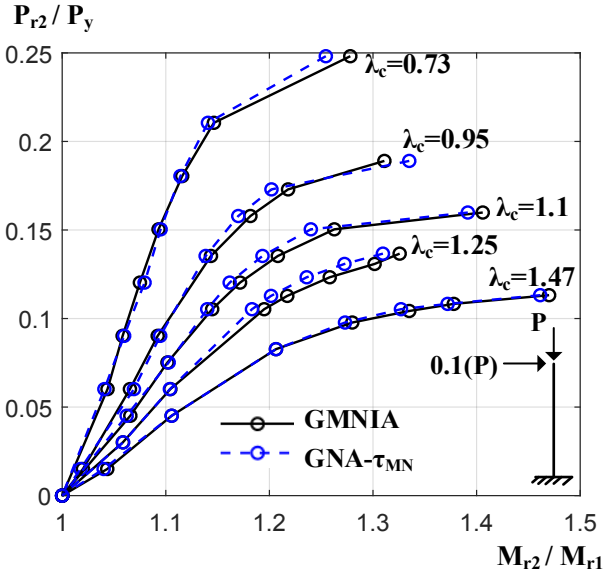

Fig.11 Comparison of the maximum second order moments predicted by GMNIA and those determined by GNA-τ_{MN} for the cantilever beam-columns

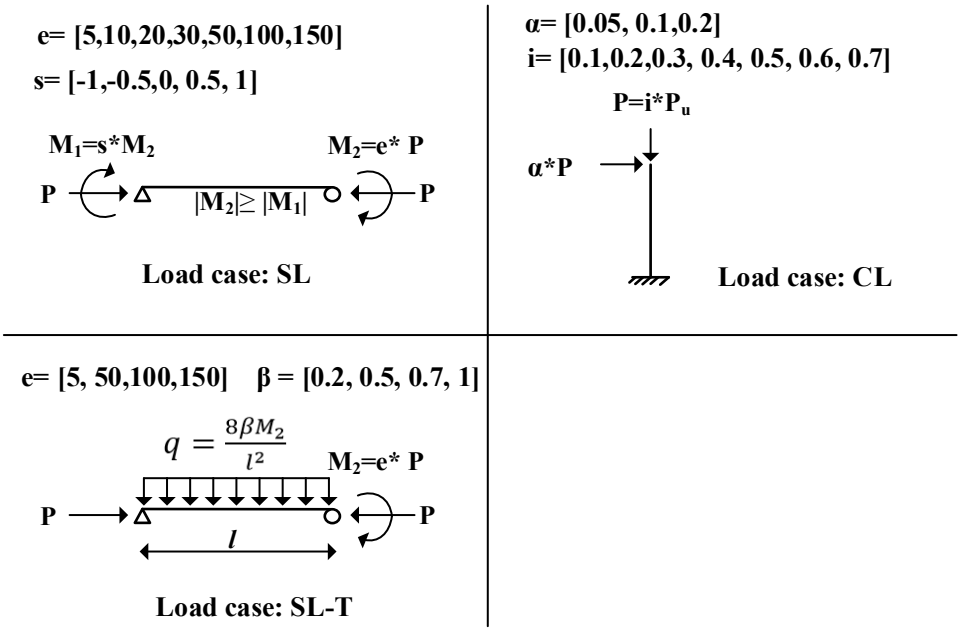

Fig.12 Load cases for the studied beam-columns

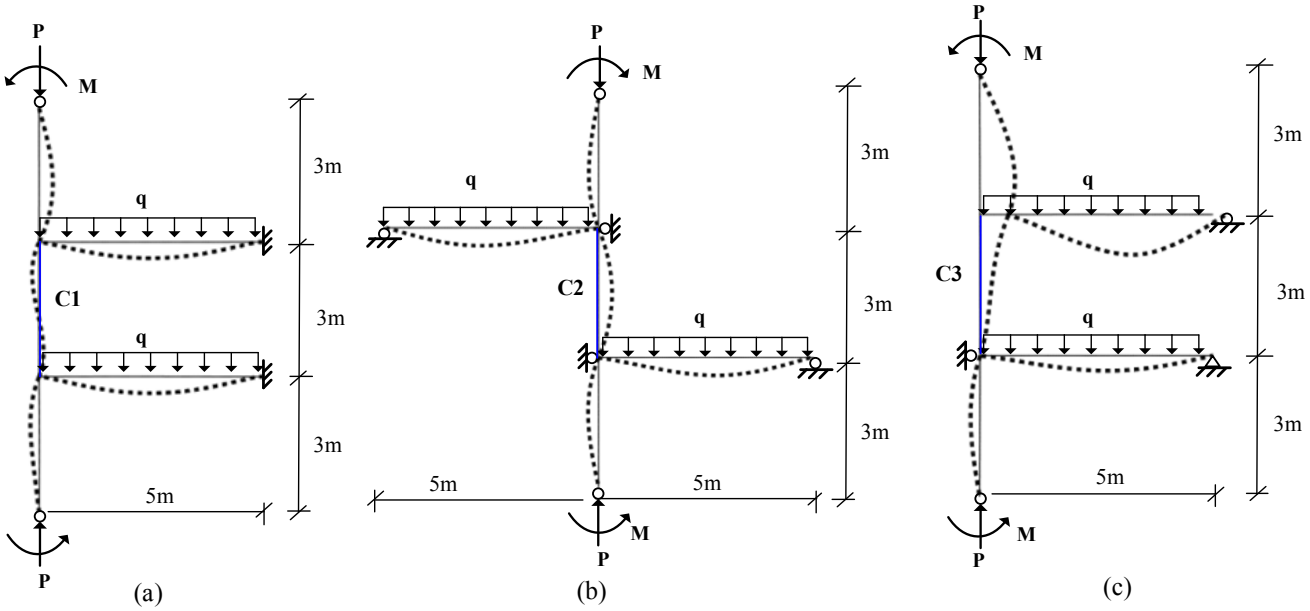

Fig. 13 Studied sub-assemblages: (a) sway-restrained beam-column with double curvature (C1) (b) sway-restrained beam-column with single curvature (C2) (c) sway-permitted beam-column with double curvature (C3)

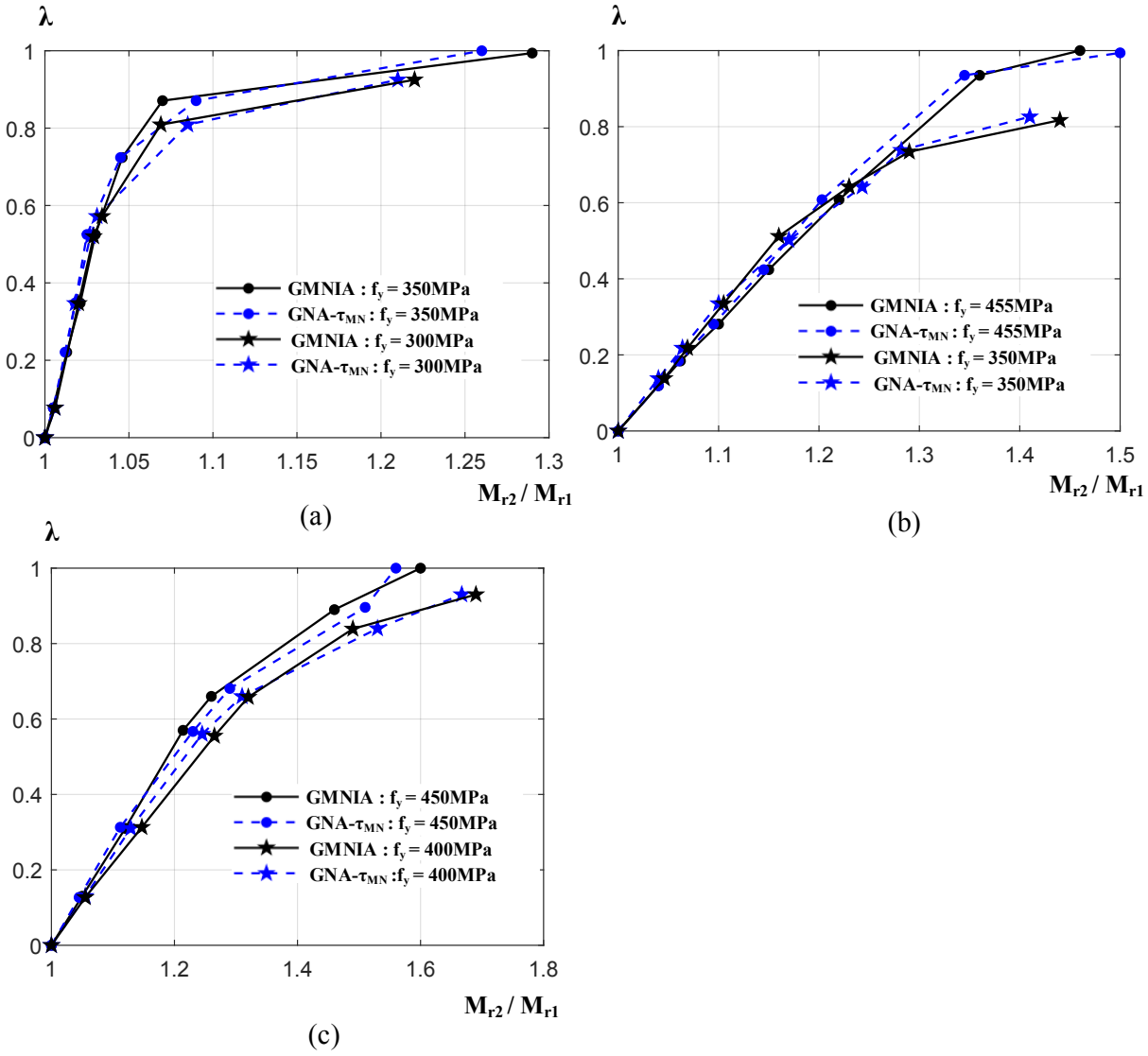

Fig.14 Comparison of the maximum second order moments predicted by GMNIA and those determined by GNA-τ_{MN} for the studied structural sub-assemblages (a) C1 (b) C2 (c) C3

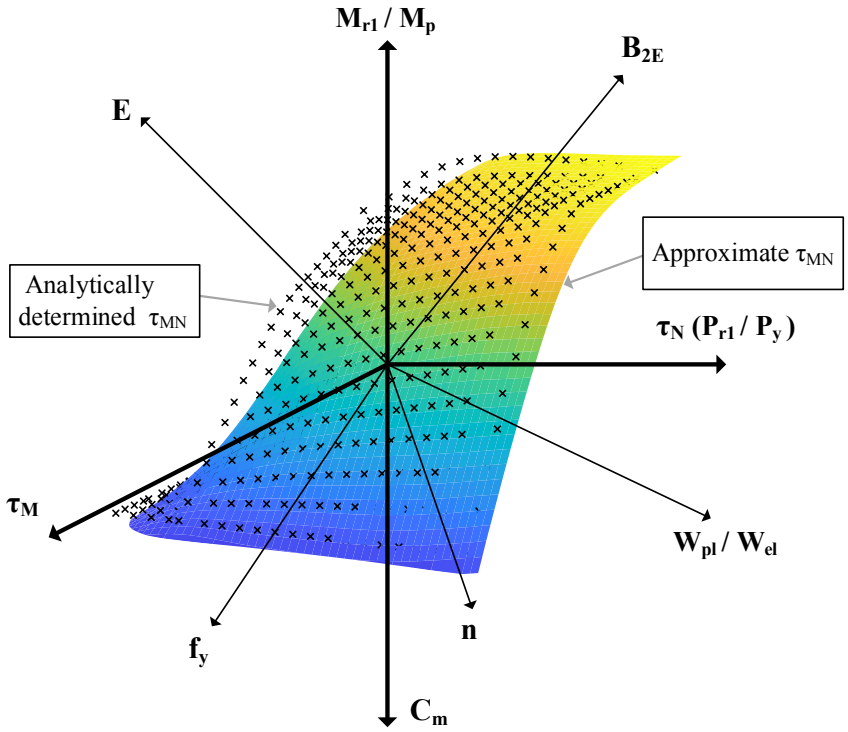

Fig.15. Illustration of developing the approximate expression for τ_{MN}

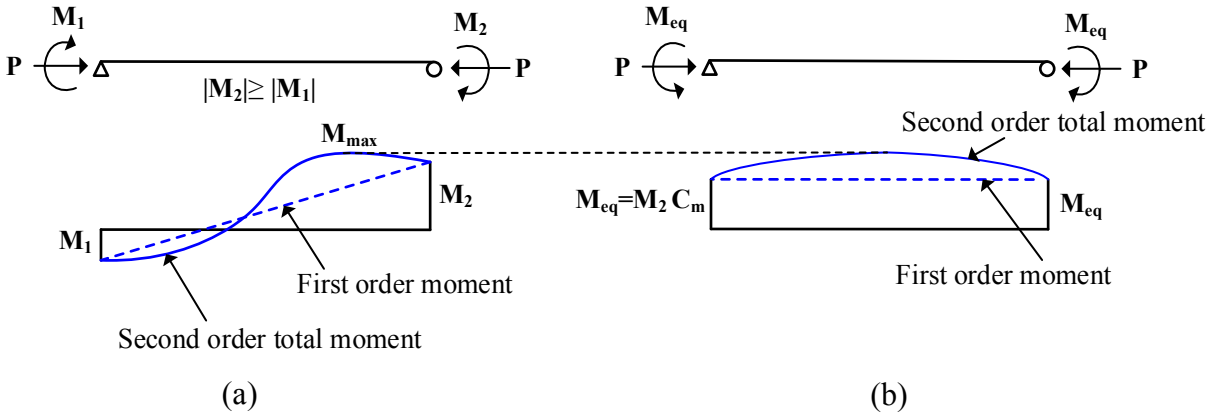

Fig. A.1 Illustration of equivalent moment

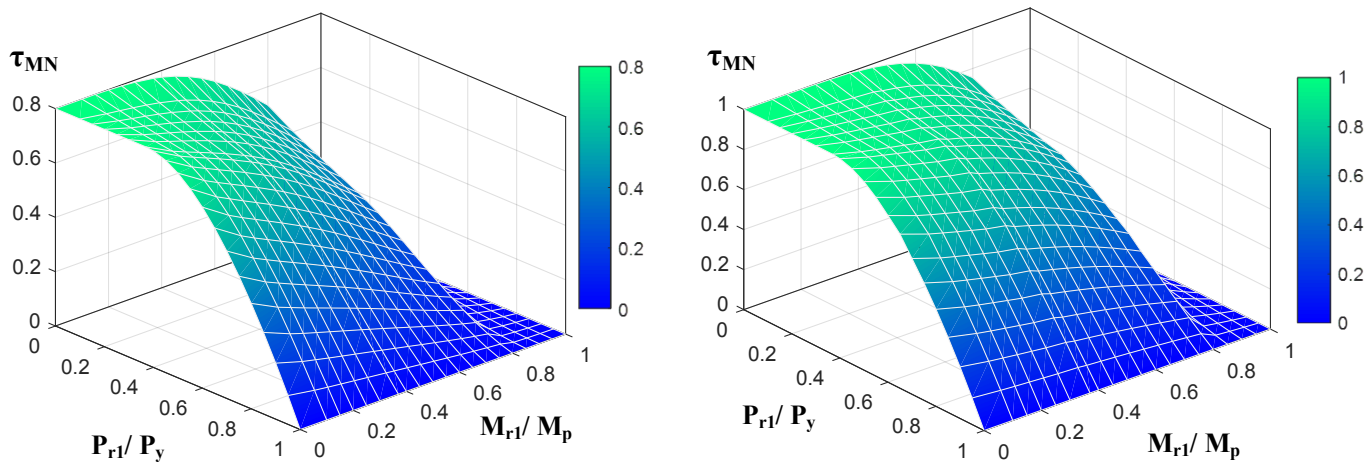

(a) (b)

Fig.16 A 3D plot of τ_{MN} for beam-columns (a) cross-section 150x100x8 (b) cross-section 150x150x10

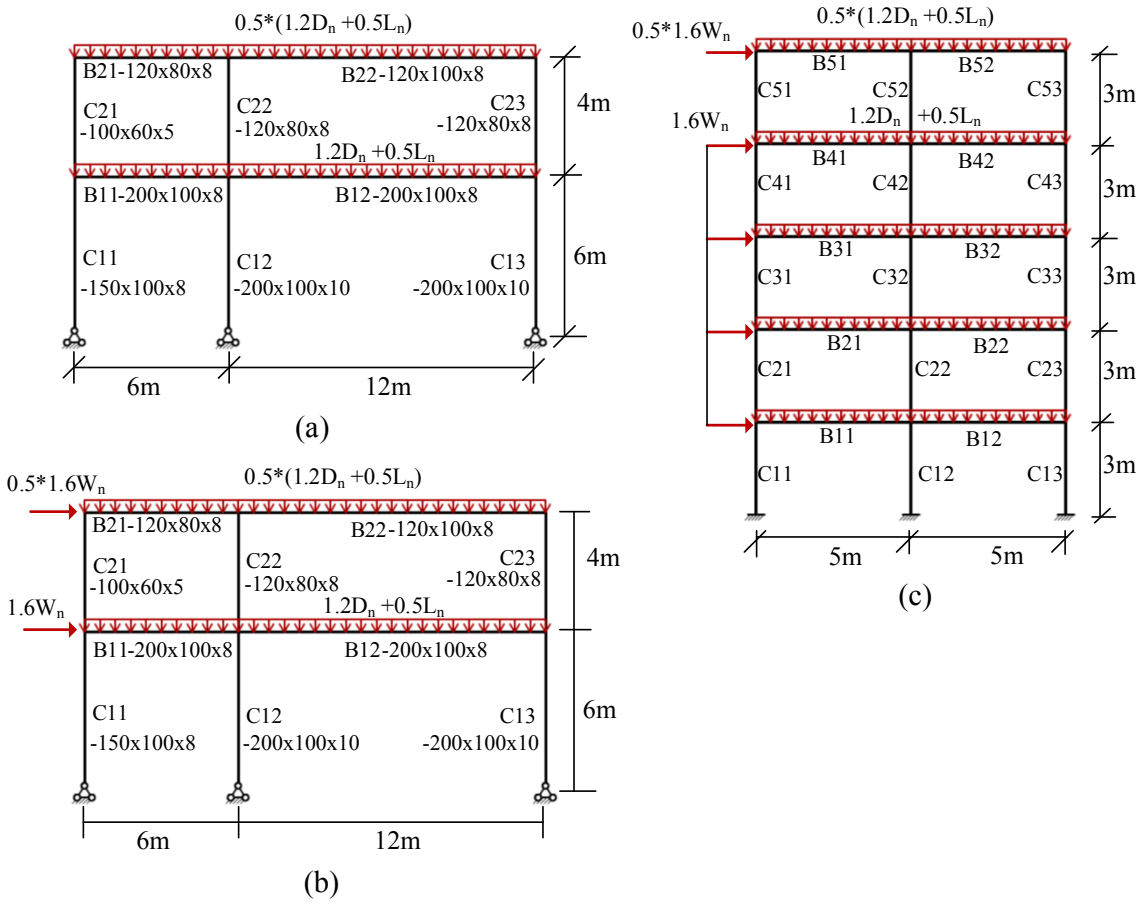

Fig.17 The studied stainless steel frames: (a) Frame-2X2-G, (b) Frame-2X2-GW, (c) Frame-2X5-GW

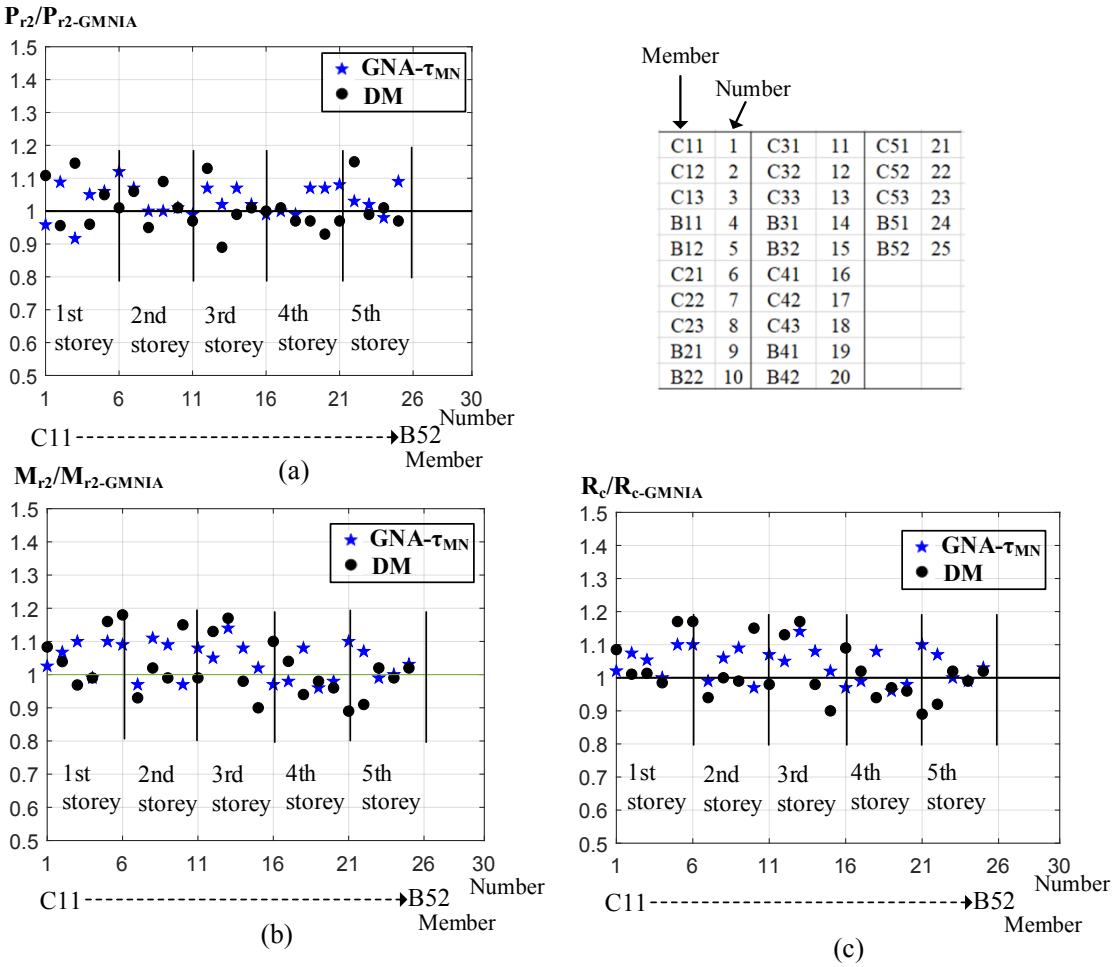

Fig.18 Comparison of the predicted results determined by different methods (a) P_{r2} determined by GNA-τ_{MN} and DM normalized by those determined by GMNIA (b) M_{r2} determined by GNA-τ_{MN} and DM normalized by those determined by GMNIA (C) R_c determined by GNA-τ_{MN} and DM normalized by those determined by GMNIA

The authors declare no conflict of interest.